*Geophysical Research Letters*

Supporting Information for

# Detailed nucleation process and mechanism of the July 2019 Mw 6.4 Ridgecrest, California earthquake

Min Liu[1,2], Miao Zhang[2*] and Hongyi Li[1*,3]

[1]School of Geophysics and Information Technology, China University of Geosciences (Beijing), Beijing, China
[2]Department of Earth and Environmental Sciences, Dalhousie University, Halifax, Nova Scotia, Canada
[3]Shanghai Sheshan National Geophysical Observatory, Shanghai, China

Corresponding author: Miao Zhang (miao.zhang@dal.ca) and Hongyi Li (lih@cugb.edu.cn)

## Contents of this file:



## Additional Supporting Information (Files uploaded separately)



## Introduction

This supporting information provides two texts, 43 figures, one table (separate from this file) and one movie (separate from this file) to support the discussions in the main text.

## Text S1. Earthquake locaiton uncertainty

Location uncertainty is essential for evaluating the confidence of earthquake locations. However, there is no standard method for assessing the uncertainty of locations obtained with waveform-based methods. To estimate the location uncertainty of foreshocks listed in the Match&Locate (M&L) catalog, we conducted a bootstrapping analysis for the two detections with the highest and lowest averaged cross-correlation (CC) values (EQ 3 with CC of 0.8851 and EQ 30 with CC of 0.3635; See event ID in Table S1), which roughly represent the best and worst location results, respectively. The principle is to repeatedly perform the M&L relocation and remove one phase (P or S) recorded at one three-component station in each round. We adopted nine stations (18 phases and 54 components) in the M&L relocation, which means the M&L relocation was repeated 18 times, with one phase removed each time. The detailed procedure was the same as step 2 of the foreshock catalog creation (see Section 2 in the main text). The results of the bootstrapping analysis indicate that the event with the highest CC value has a location uncertainty of approximately 3 m, both horizontally and vertically, and the event with the lowest CC value has a slightly larger location uncertainty, of 8 m horizontally and 10 m vertically (Figure S4). We assumed the location uncertainty of the other foreshocks was within the range of these two events. Thus, our horizontal and vertical location uncertainties are 3–8 m and 3–10 m, respectively.

Following Zhang and Wen (2015a), we show the plan-view CC convergence and waveform comparison between each event with the template event ($M_L$ 1.5) after relatively travel-time correction based on their location difference (Figure S5-43).

## Text S2. Estimation of rupture radius from local magnitude

We estimated the rupture dimensions for the $M_L$1.5 and $M_L$ 2.15 events based on their local magnitude ($M_L$) and a simple circular crack model. We first converted the $M_L$ to the scalar moment ($M_0$) based on the moment-magnitude relationship (Abercrombie, 1996) in the region, as below:

$$\log(M_0) = 9.8 + M_L \qquad (1)$$

We then estimated the rupture radius $r$ from $M_0$, based on a simple circular crack model and the scaling relationship proposed by Kanamori & Anderson (1975) :

$$r = \left(\frac{7M_0}{16\Delta\sigma}\right)^{1/3} \qquad (2)$$

Here, an empirical stress drop ($\Delta\sigma$) of 3 MPa was adopted in the calculation of the rupture radius (Yoon et al., 2019). Thus, the rupture radiuses of the $M_L$1.5 and $M_L$ 2.15 events were 31 m and 50 m, respectively.

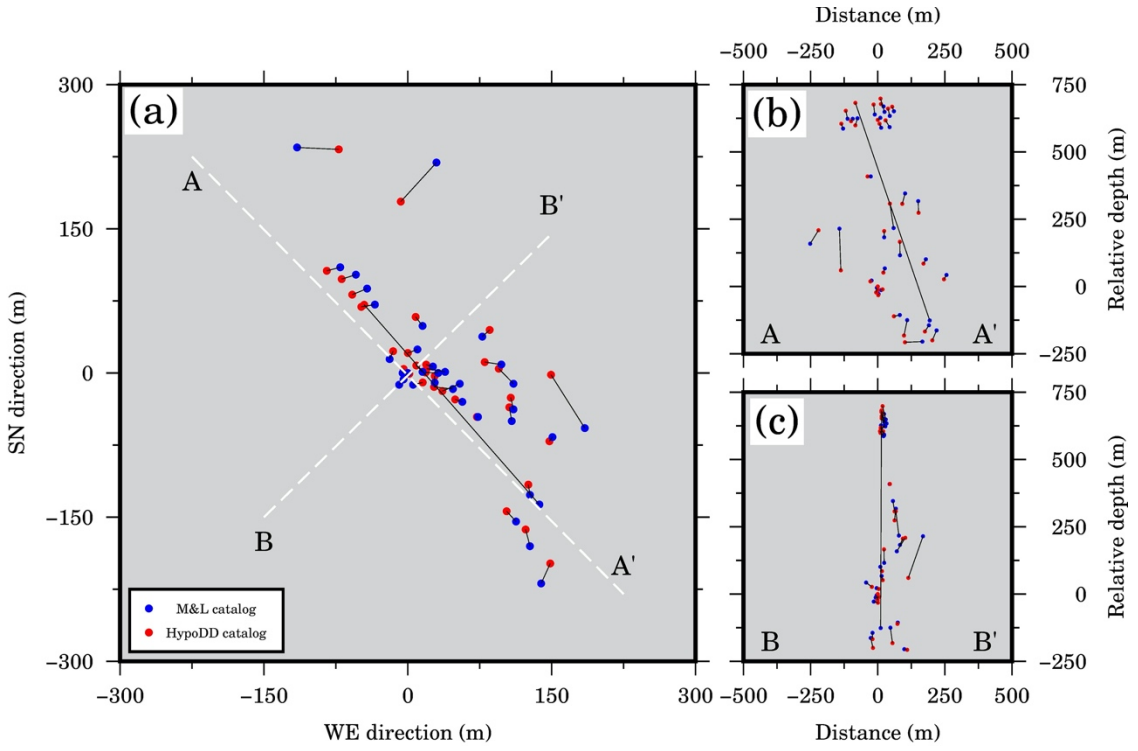


**Figure S1**. (a) Plan-view comparison of locations of the 35 foreshocks common to both the M&L catalog (blue dots) and the hypoDD catalog (red dots). Event locations are relative to the hypocenter of the $M_L$ 1.5 event. The corresponding event-pairs in the two catalogs are connected by black lines. (b) Similar to (a), but for the cross-section along AA', which corresponds to one of the fault planes of the $M_L$ 4.0 foreshock. (c) Similar to (b), but for the cross-section along BB'. The event-pair with a large location difference is further analyzed in Figure S2.

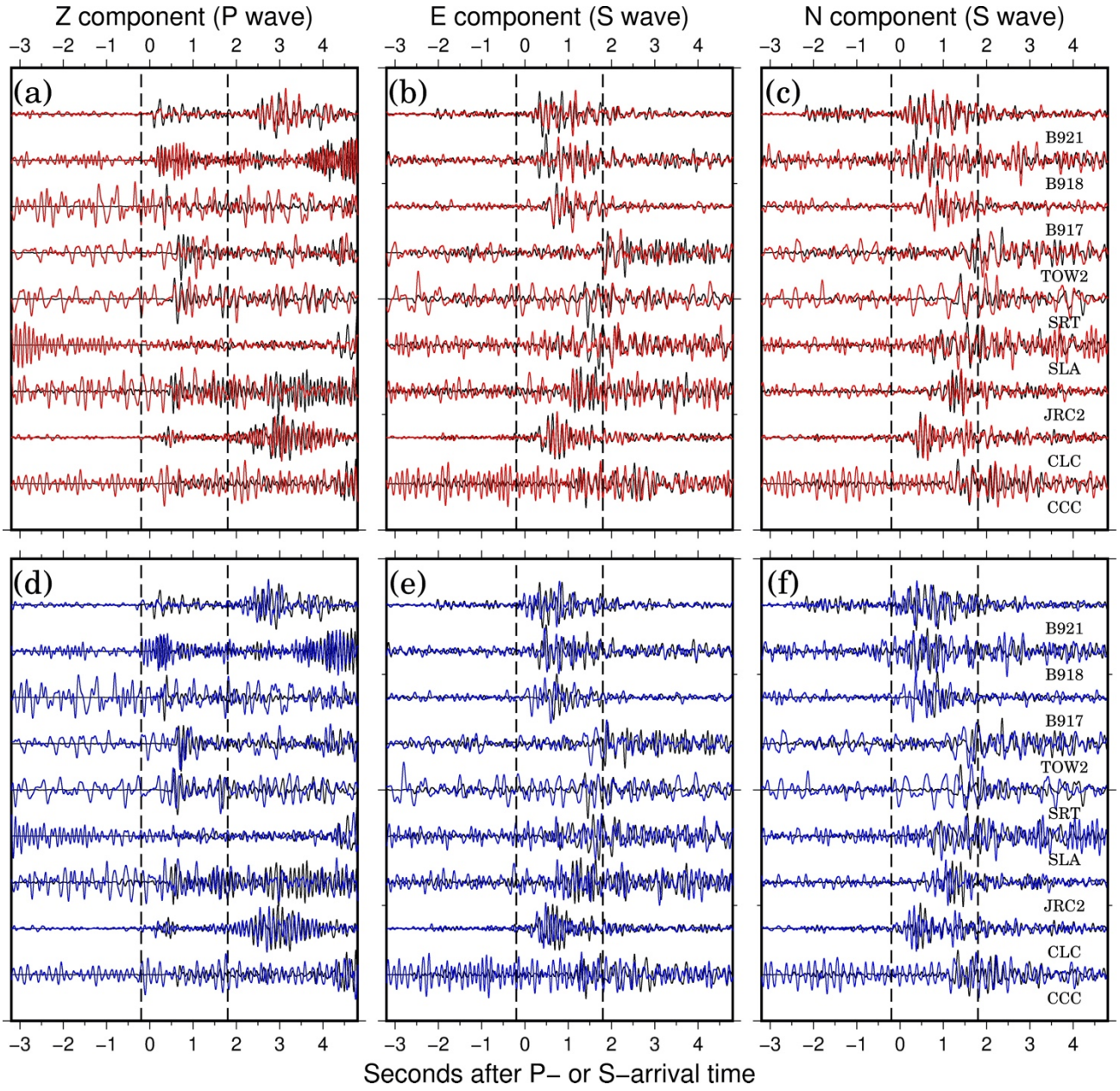


**Figure S2**. Investigation of the location reliability for the event pair with large location difference in Figure S1 (see main text). We allocated the corresponding locations and origin times, listed in the M&L and hypoDD catalogs, to the event, and compared its waveforms with the $M_L$ 1.5 event after location correction. (a–c) Red and black waveforms represent the three-component seismograms of the event located by M&L and the reference event ($M_L$ 1.5), respectively. The two black dashed lines highlight the template windows used in the M&L method. (d-f) Similar to (a–c), but for the hypoDD location. Clearly, the event was mislocated in the hypoDD catalog.

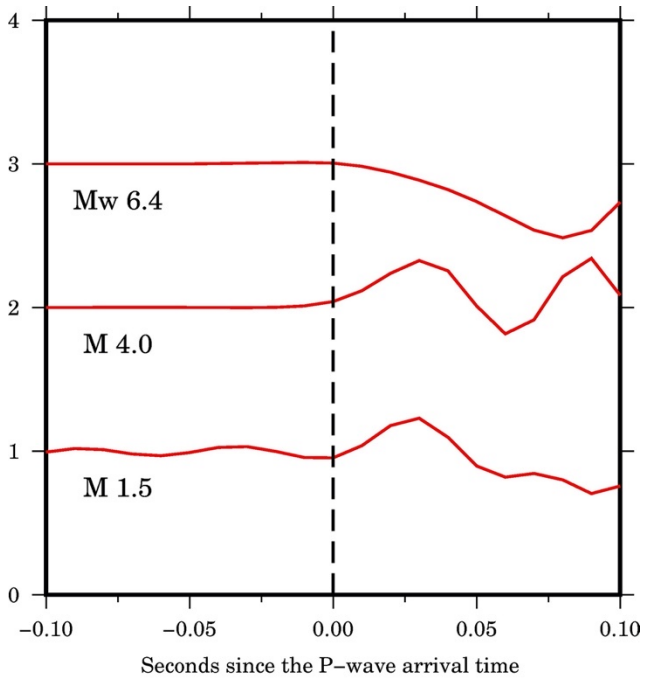


**Figure S3**. Comparison of the early P phases between the $M_L$ 1.5, $M_L$ 4.0 foreshocks, and the Mw 6.4 mainshock. All traces were aligned at the manual P first arrivals.

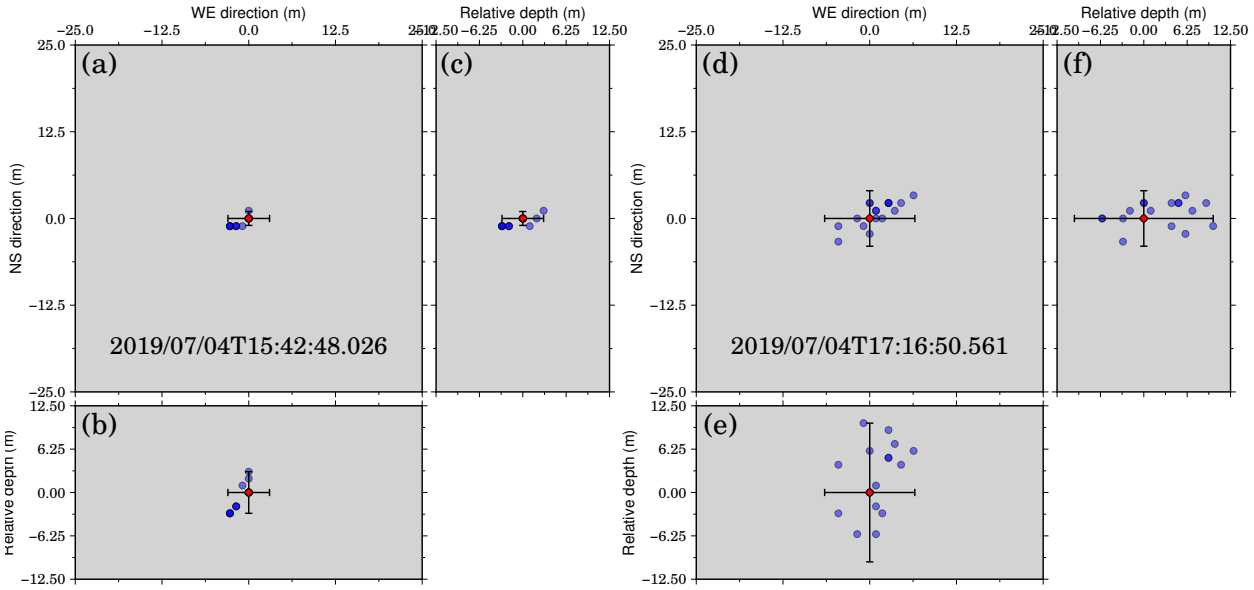


**Figure S4**. Location uncertainty of the two events with the highest and lowest CC values. (a) Red diamonds represent the epicentral location of the event located with the M&L method with the highest CC value (EQ 3 with a CC of 0.8851; See event ID in Table S1). Blue dots indicate the relocations based on the bootstrapping analysis. Blueness is proportional to the number of overlapping locations. The black error bar indicates the horizontal location uncertainty revealed by the bootstrapping analysis. (b–c) Similar to (a) but for the two cross-sections along the WE and NS directions. Black error bars represent the vertical location uncertainty. (d-e) Similar to (a-c) but for the event with the lowest CC value (EQ 30 with CC of 0.3635; See event ID in Table S1).

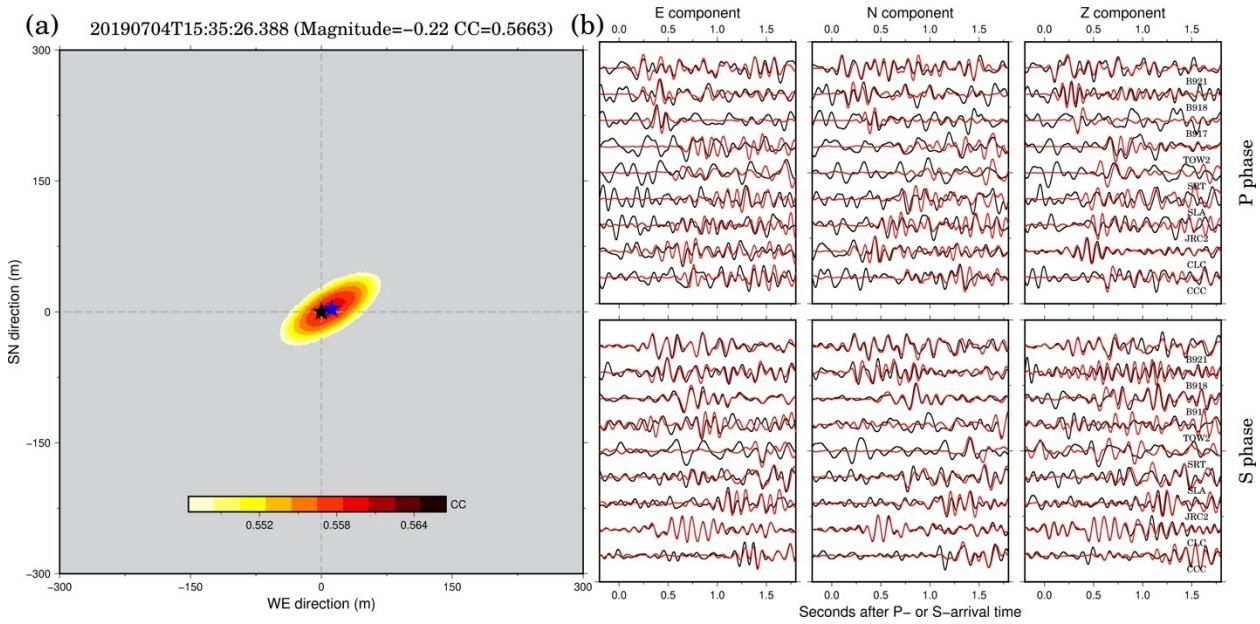


**Figures S5**. Horizontal CC convergence of EQ 1 (see event ID in Table S1) and its waveform comparison with the template event ($M_L$ 1.5). (a) Black and blue stars represent the epicenters of the template and detected events, respectively. The distribution of averaged CC coefficients is shown with a color bar. (b) Waveform comparison of P phases (top panel) and S phases (bottom panel) between EQ 1 (red) and template (black) event, from nine three-component stations after relative travel time correction.

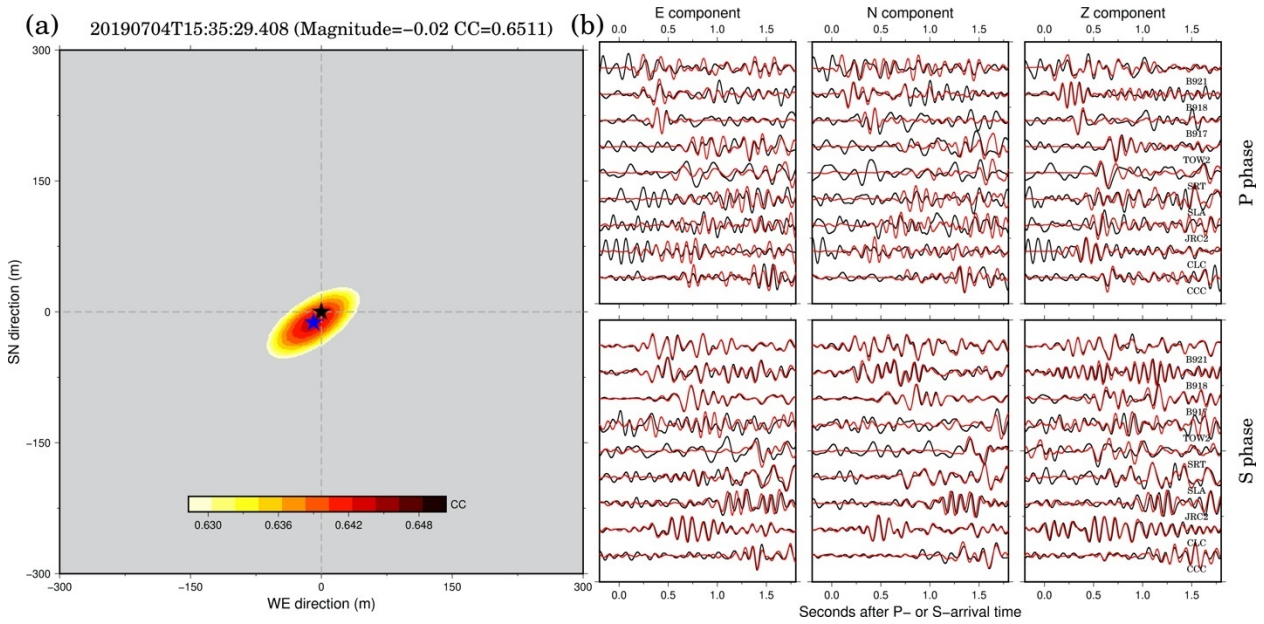


**Figures S6.** Smilar to Figure S5, but for EQ 2.

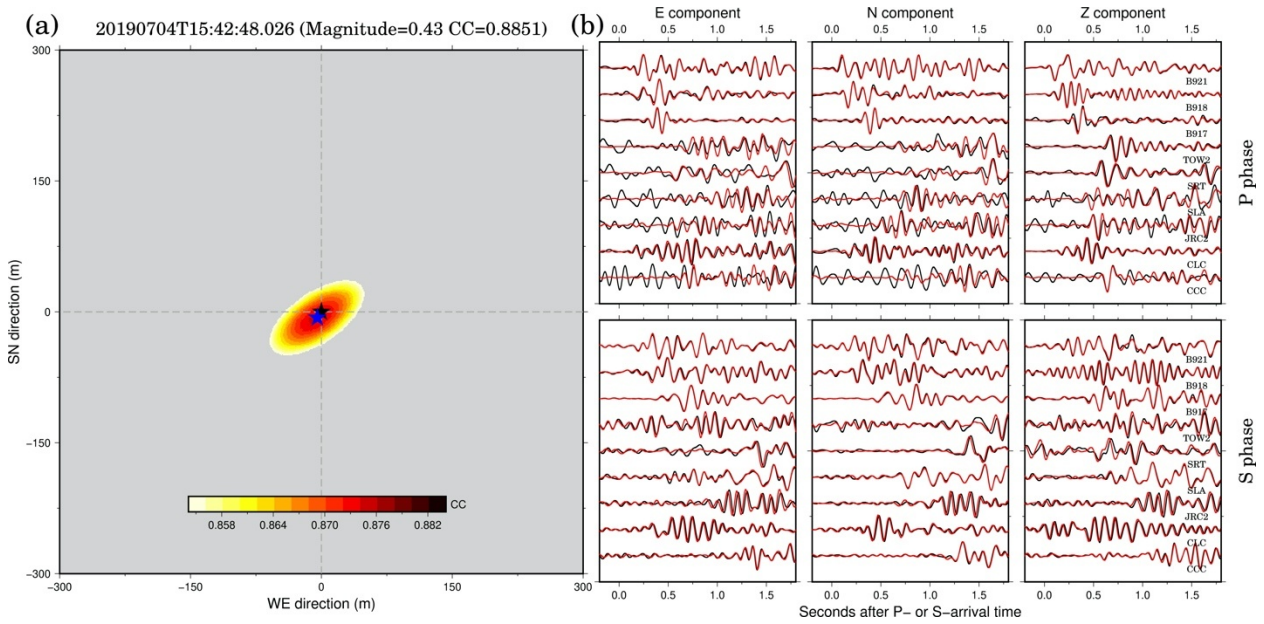


**Figures S7.** Smilar to Figure S5, but for EQ 3.

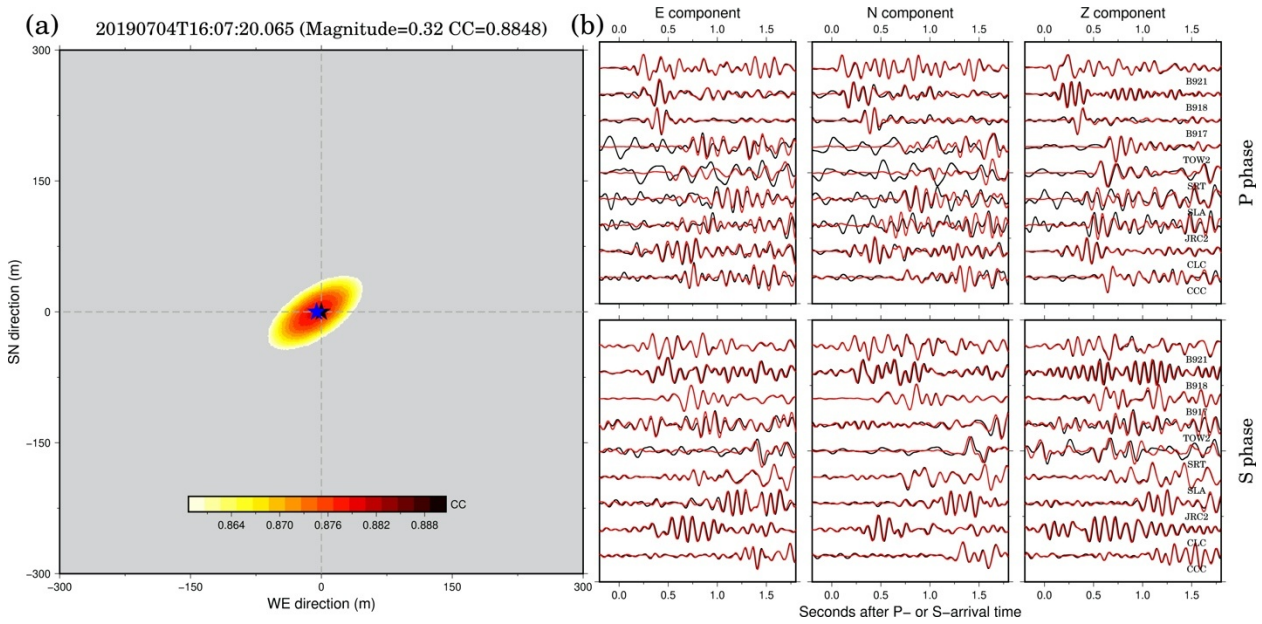


**Figures S8.** Smilar to Figure S5, but for EQ 4.

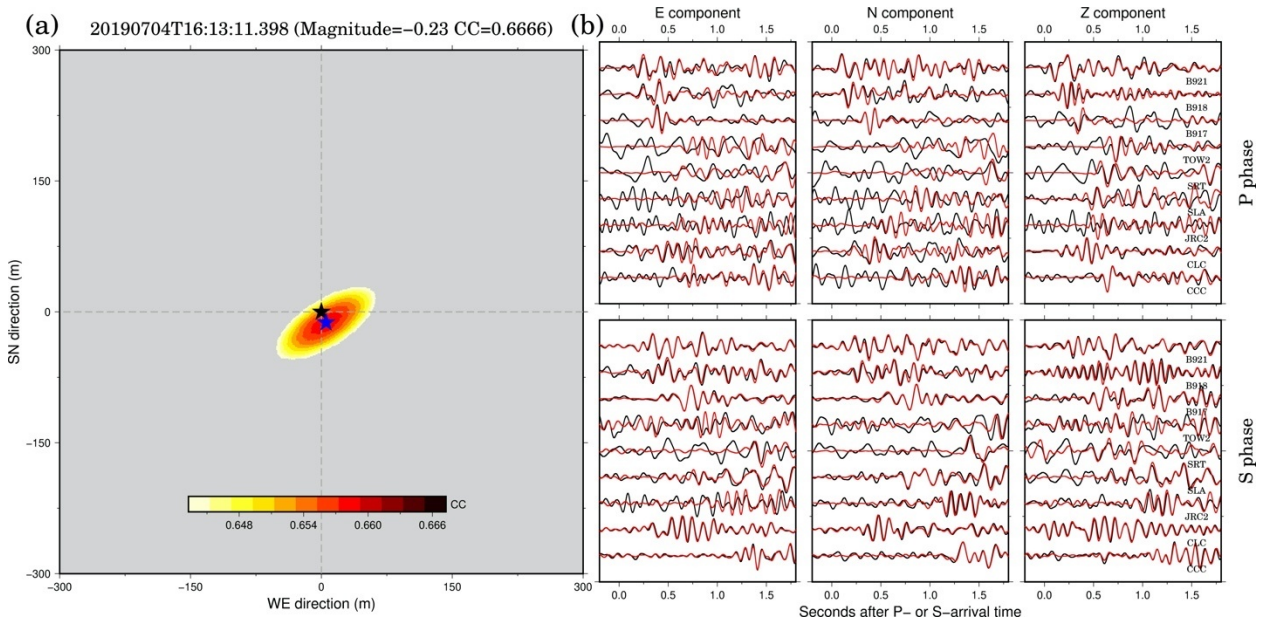


**Figures S9.** Smilar to Figure S5, but for EQ 5.

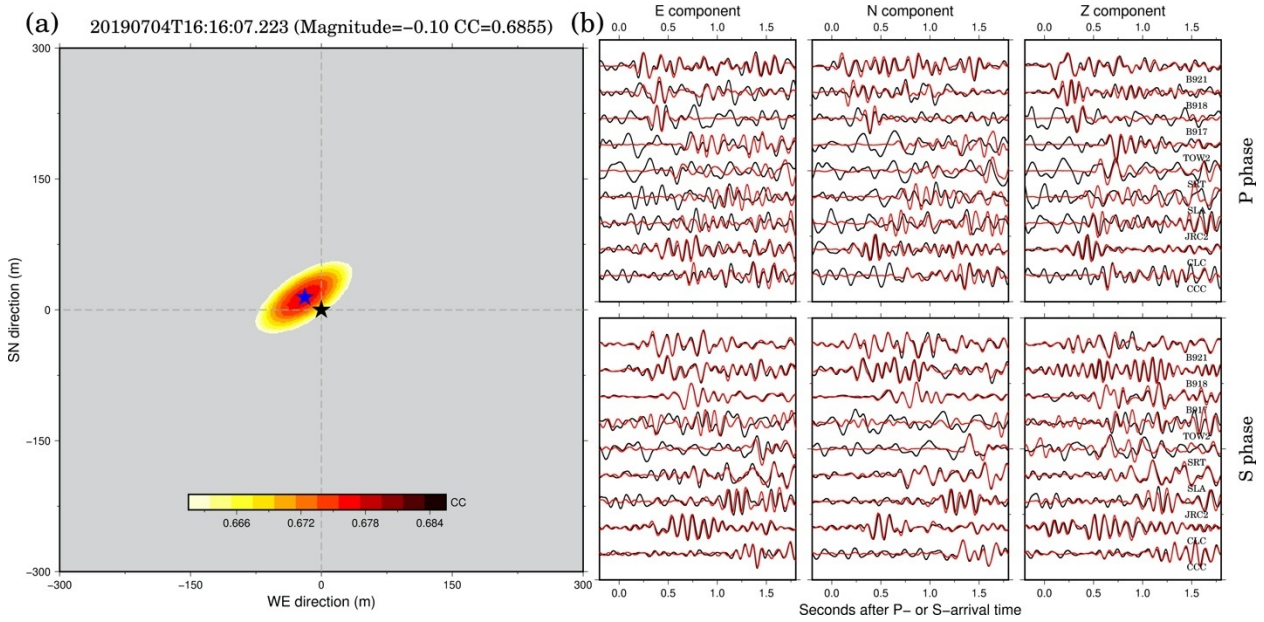


**Figures S10.** Smilar to Figure S5, but for EQ 7.

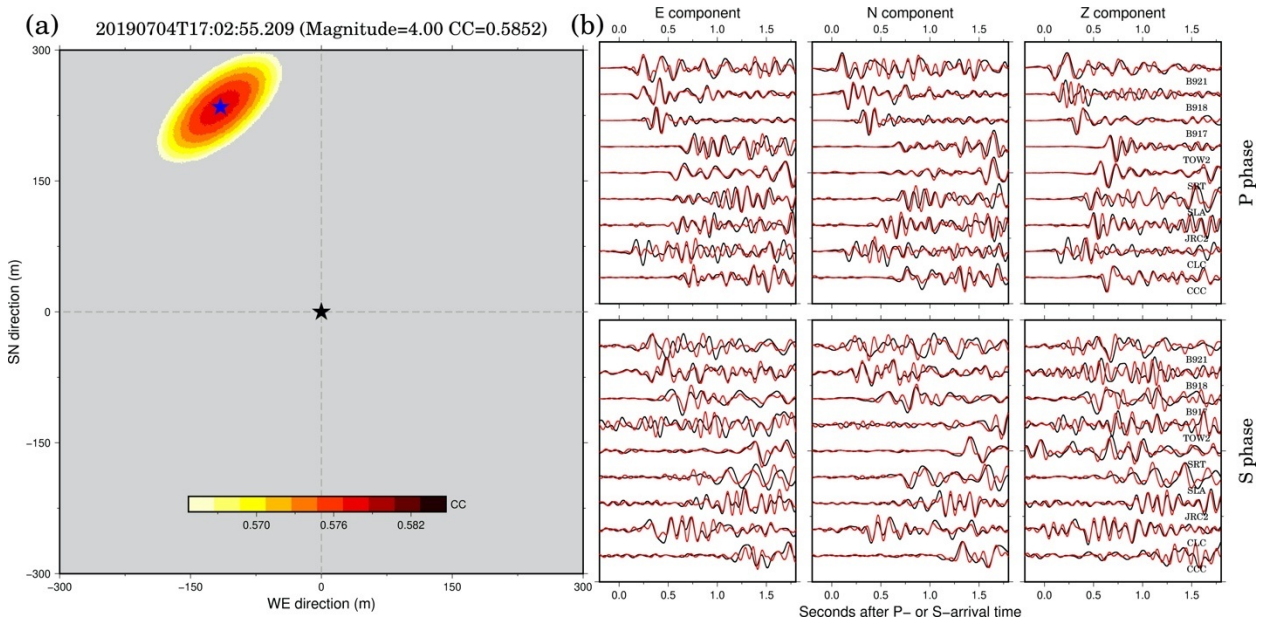


**Figures S11.** Smilar to Figure S5, but for EQ 8.

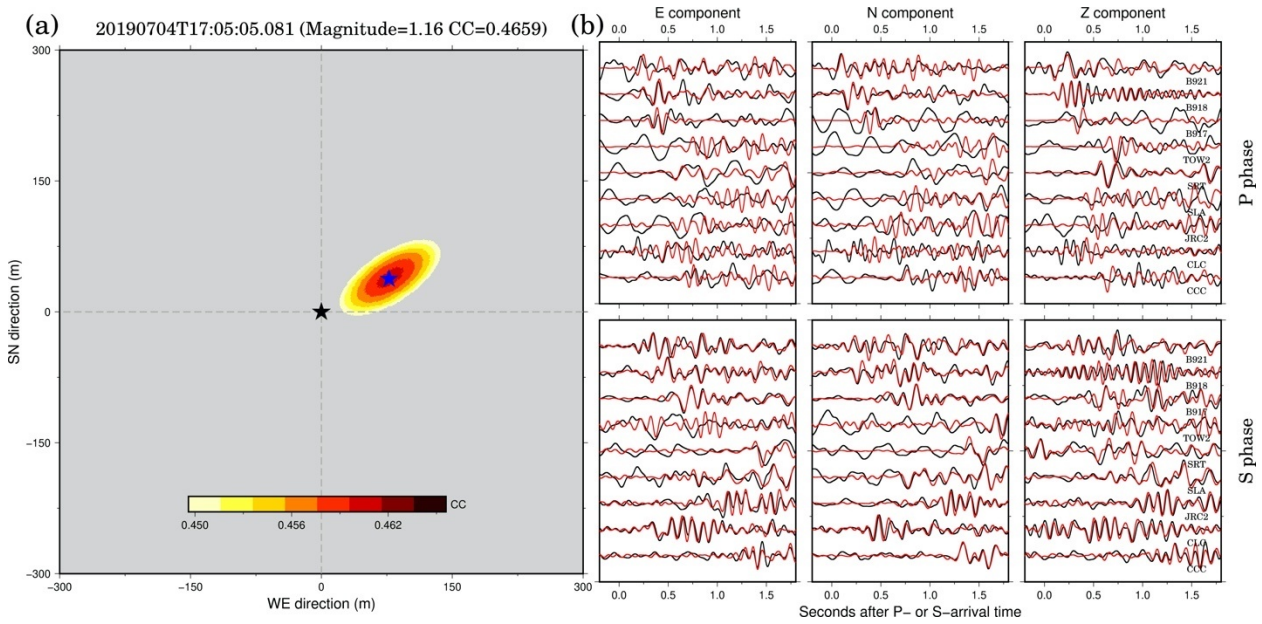


**Figures S12.** Smilar to Figure S5, but for EQ 9.

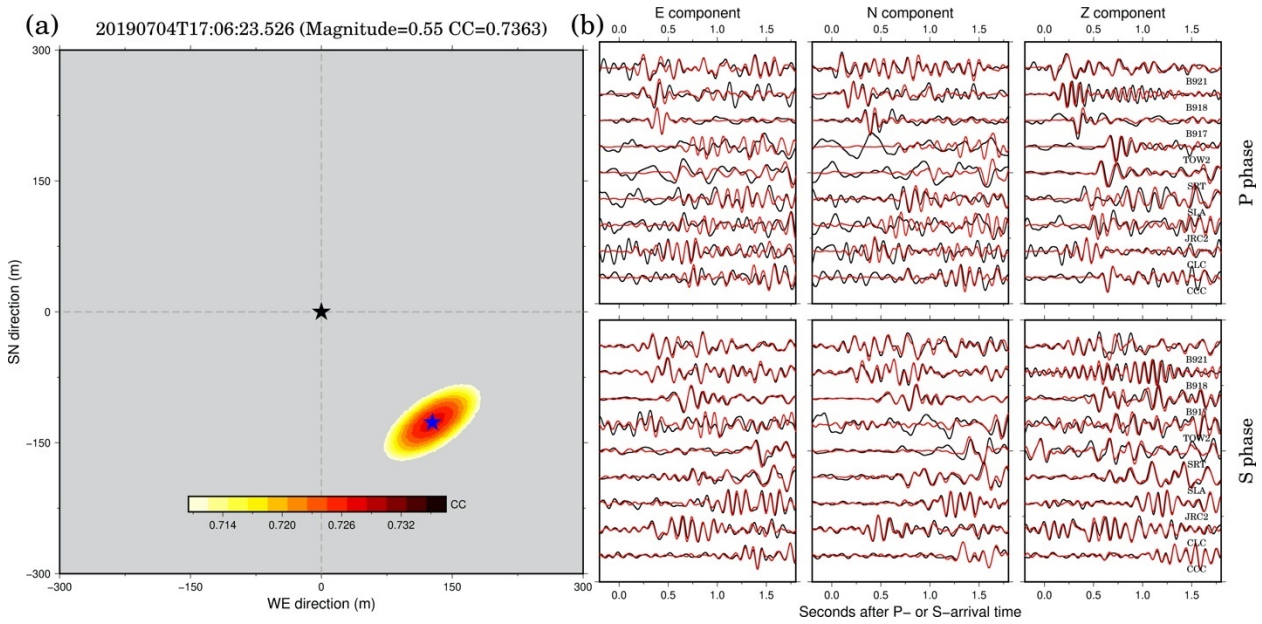


**Figures S13.** Smilar to Figure S5, but for EQ 10.

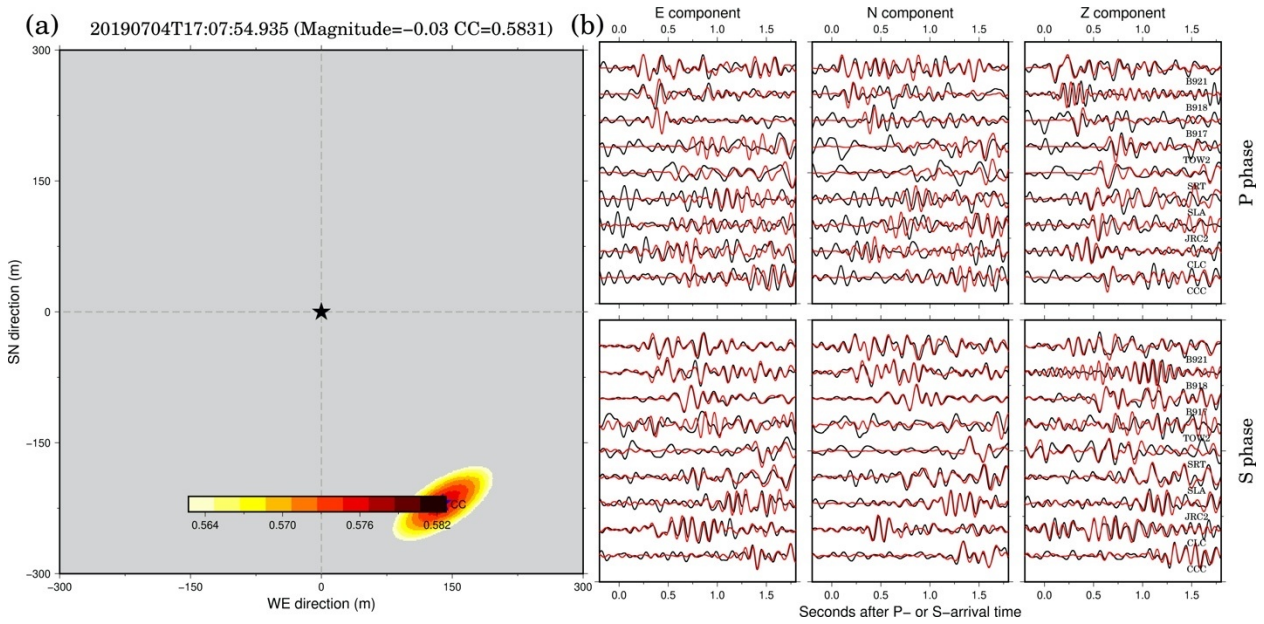


**Figures S14.** Smilar to Figure S5, but for EQ 11.

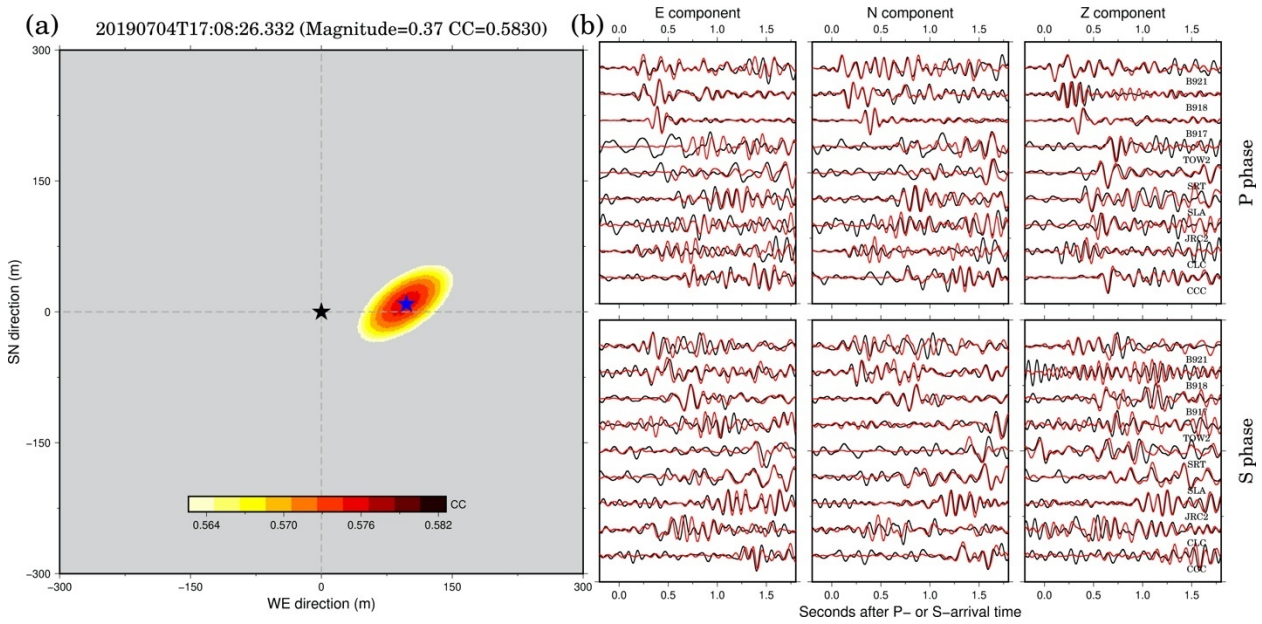


**Figures S15.** Smilar to Figure S5, but for EQ 12.

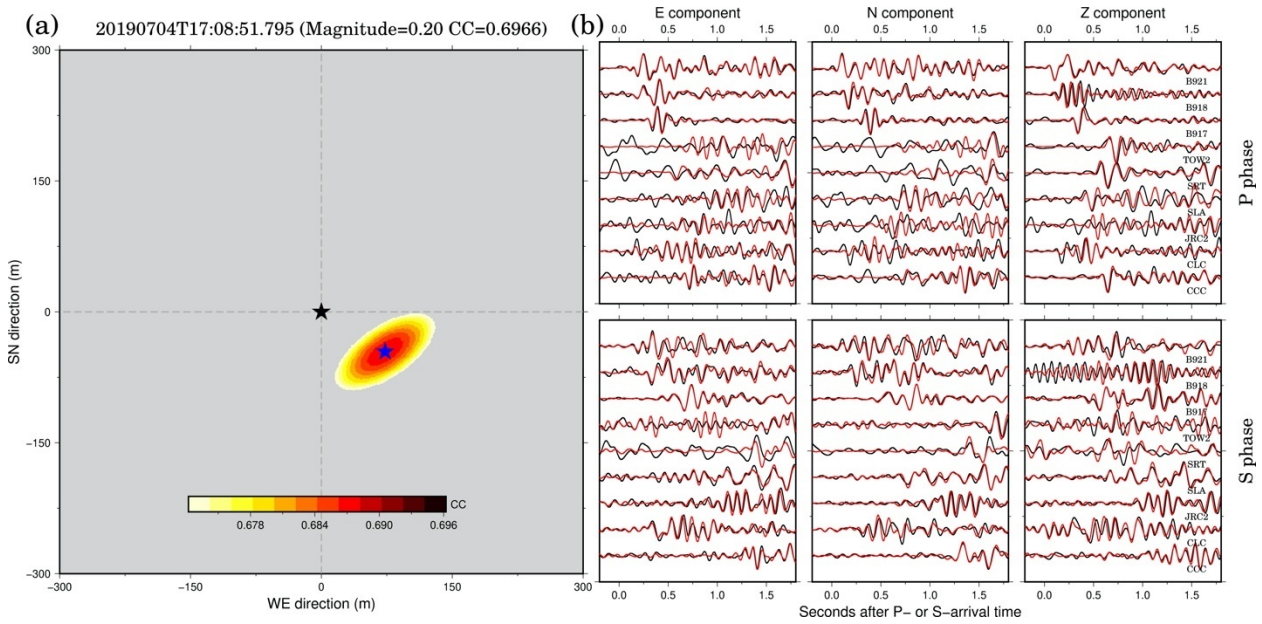


**Figures S16.** Smilar to Figure S5, but for EQ 13.

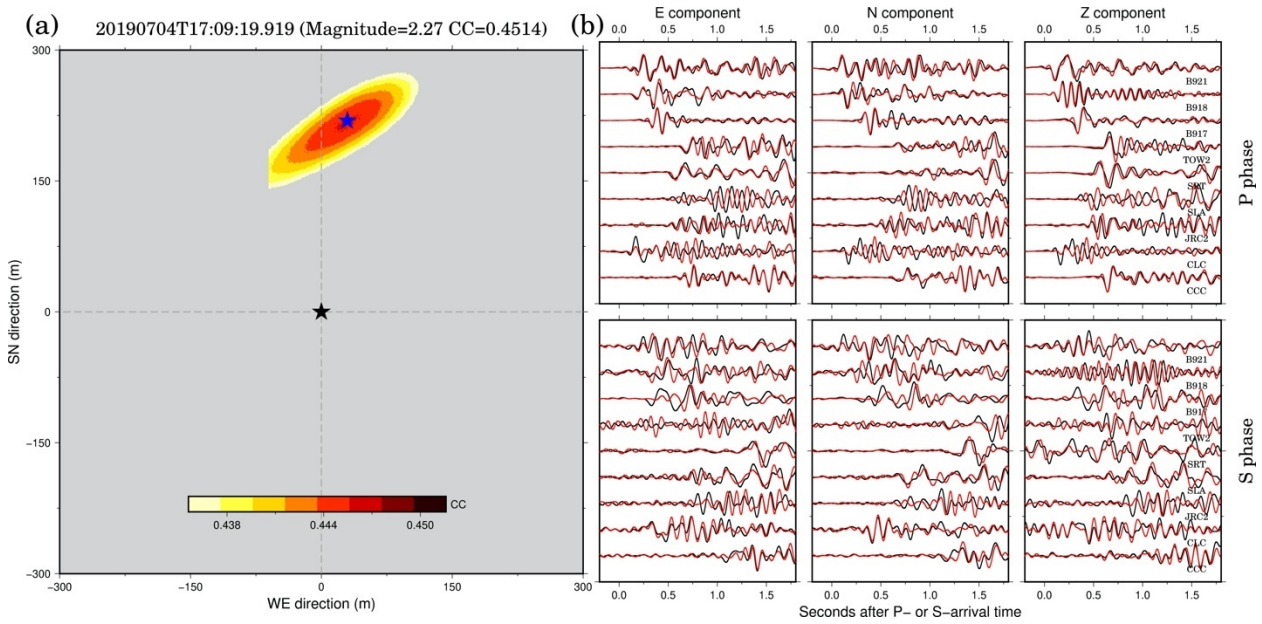


**Figures S17.** Smilar to Figure S5, but for EQ 14.

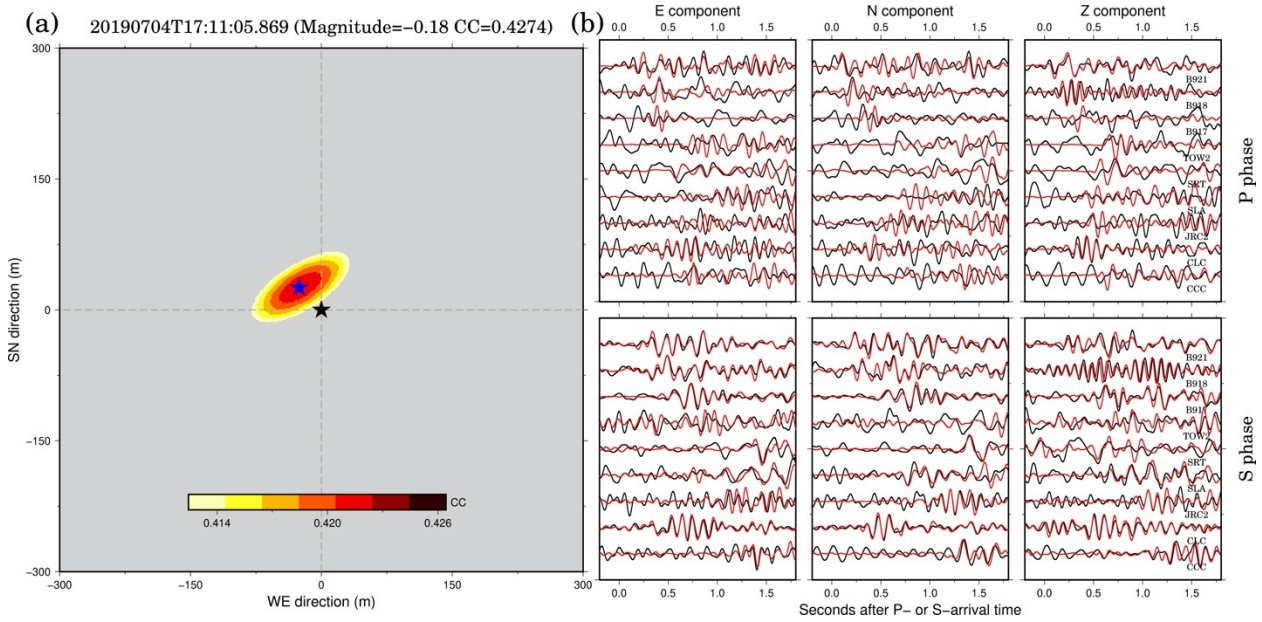


**Figures S18.** Smilar to Figure S5, but for EQ 15.

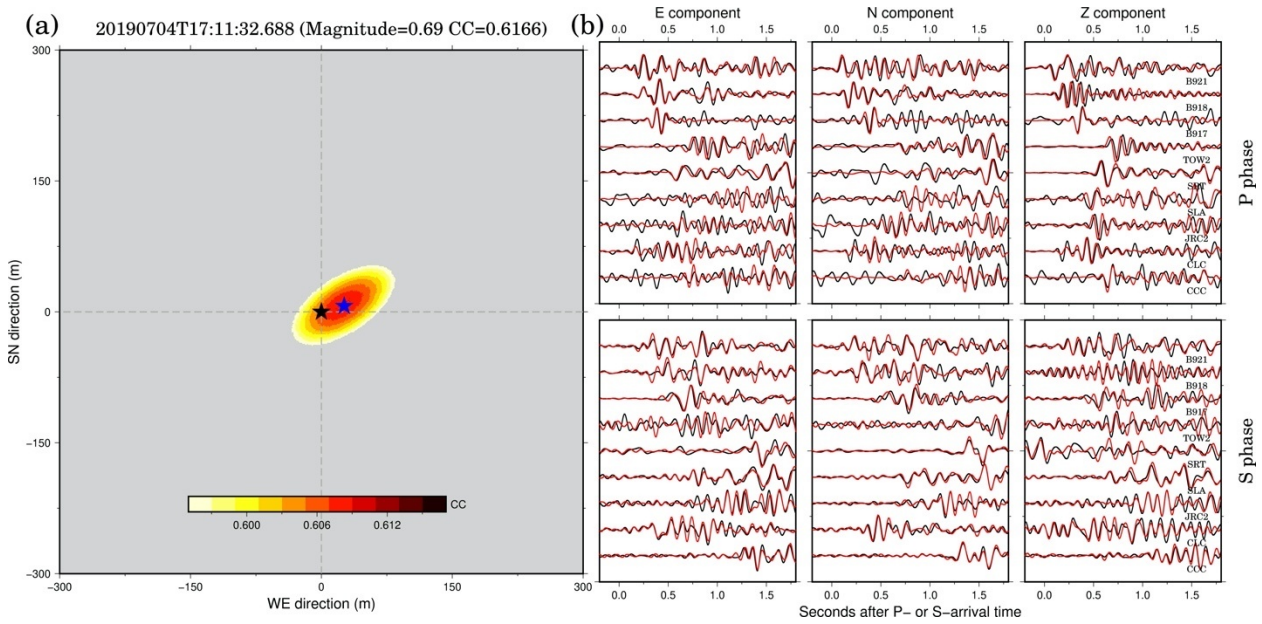


**Figures S19.** Smilar to Figure S5, but for EQ 16.

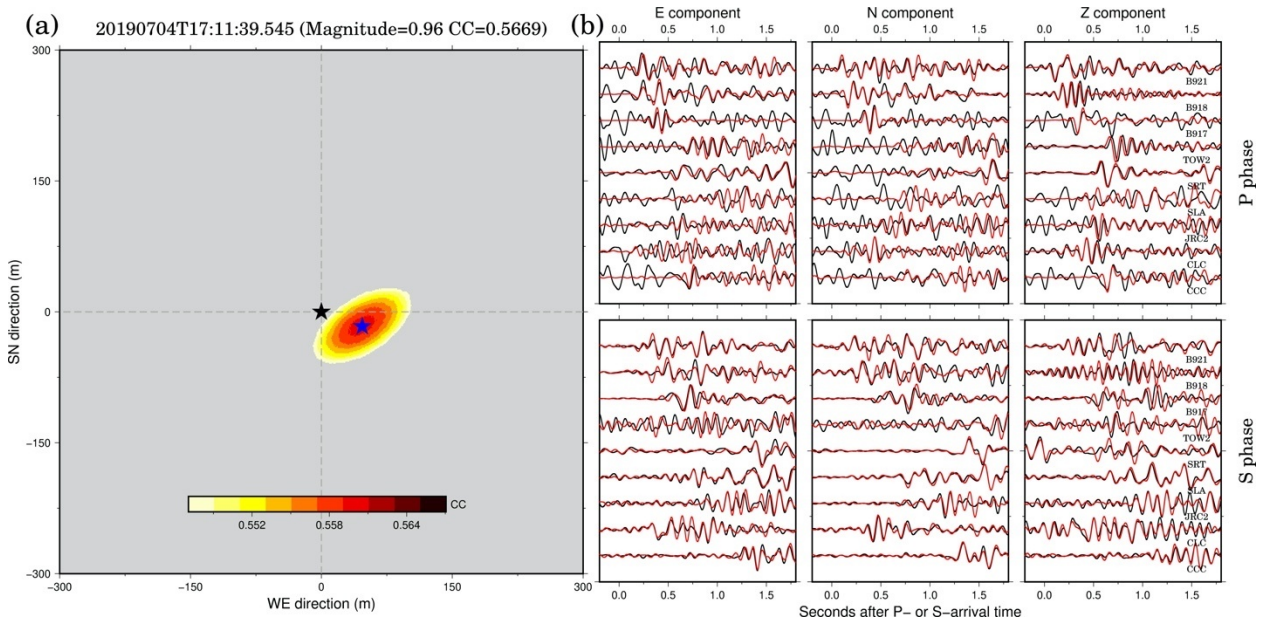


**Figures S20.** Smilar to Figure S5, but for EQ 17.

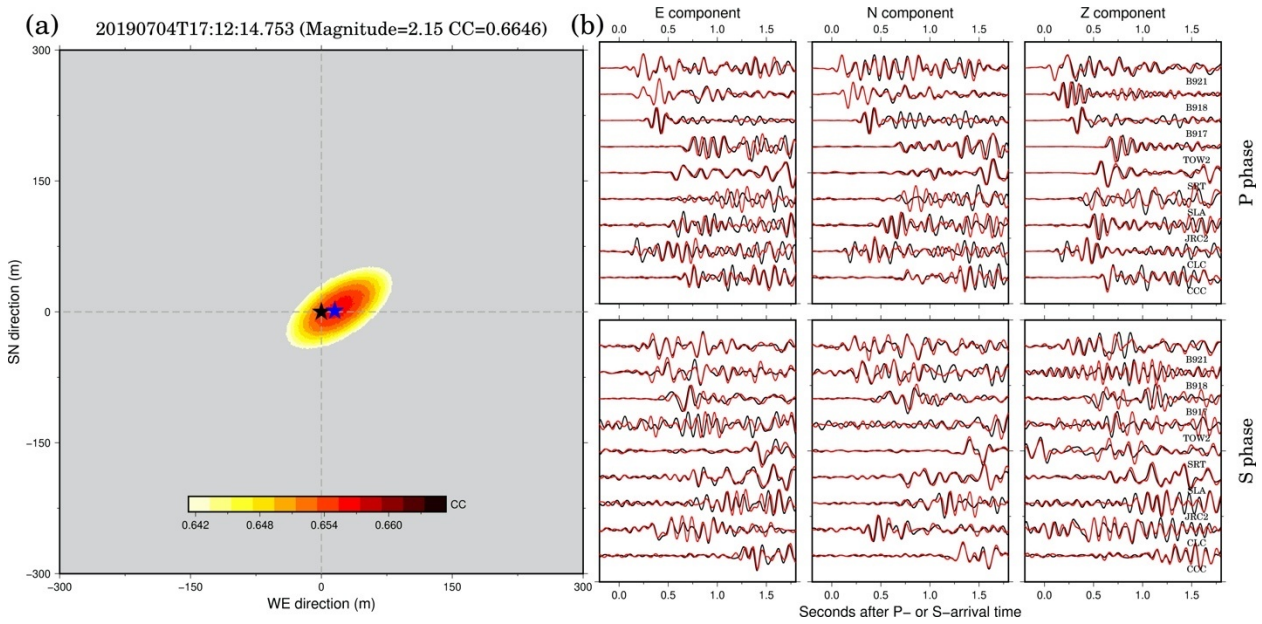


**Figures S21.** Smilar to Figure S5, but for EQ 18.

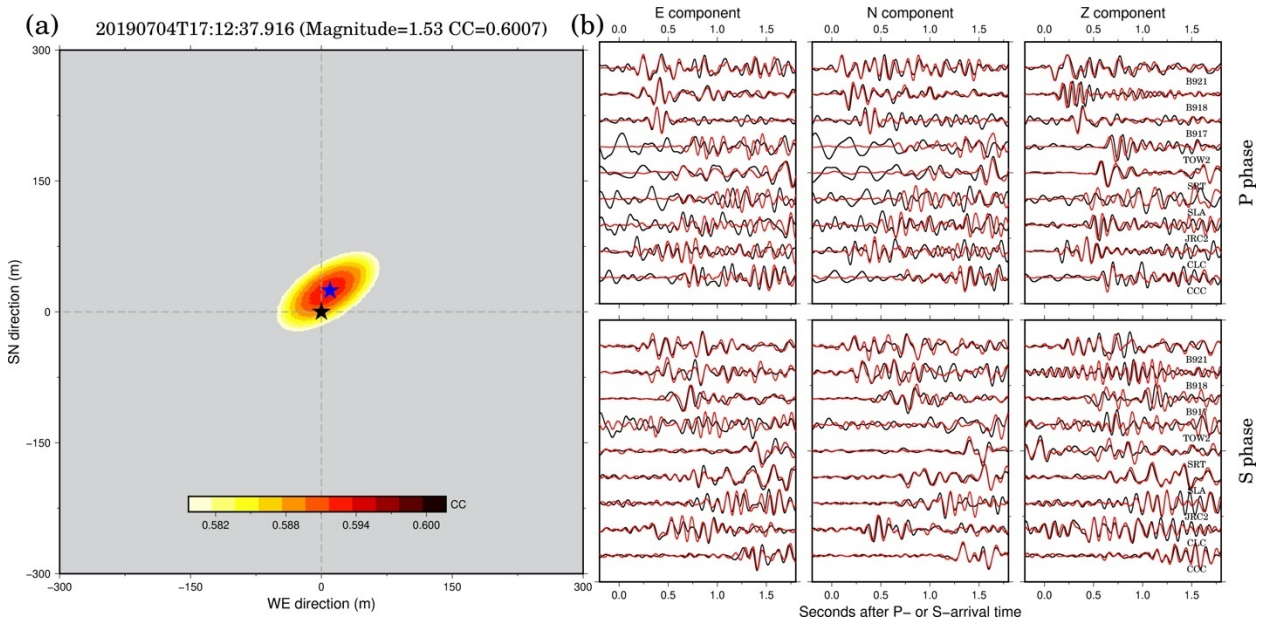


**Figures S22.** Smilar to Figure S5, but for EQ 19.

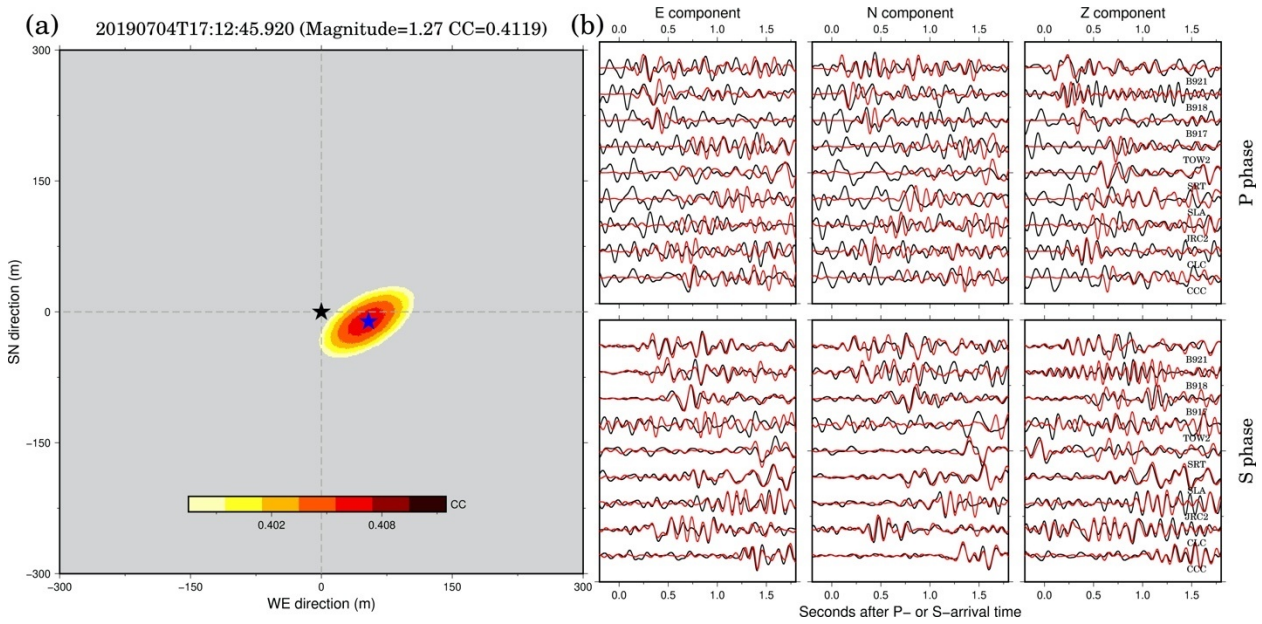


**Figures S23.** Smilar to Figure S5, but for EQ 20.

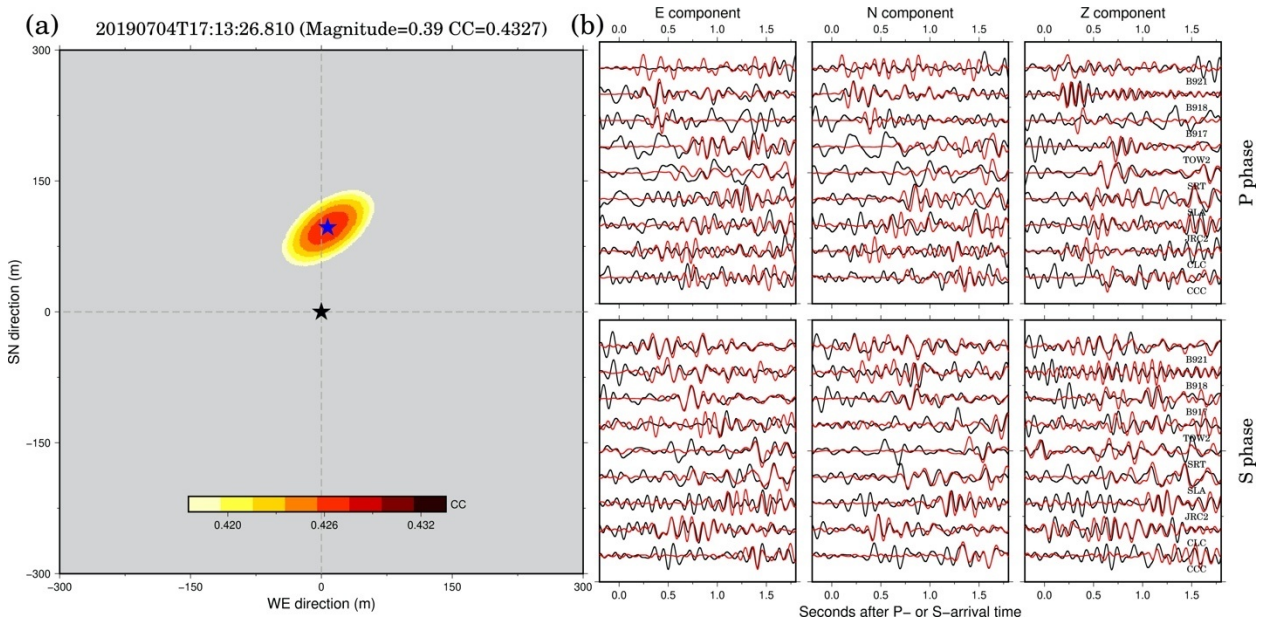


**Figures S24.** Smilar to Figure S5, but for EQ 21.

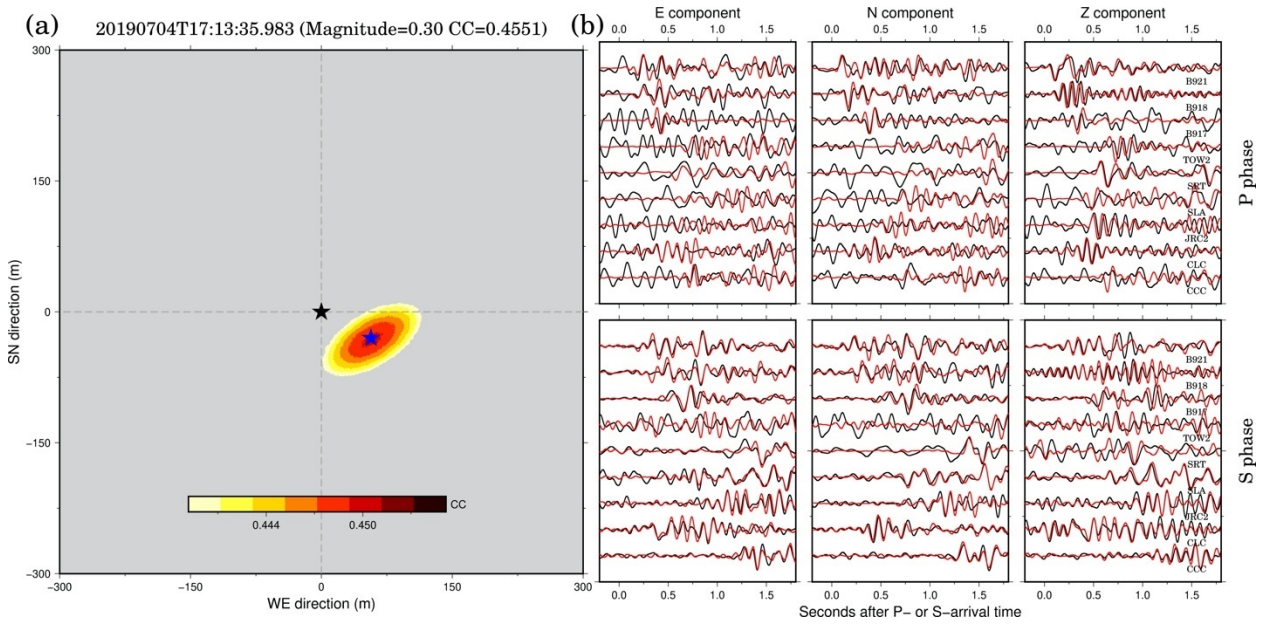


**Figures S25.** Smilar to Figure S5, but for EQ 22.

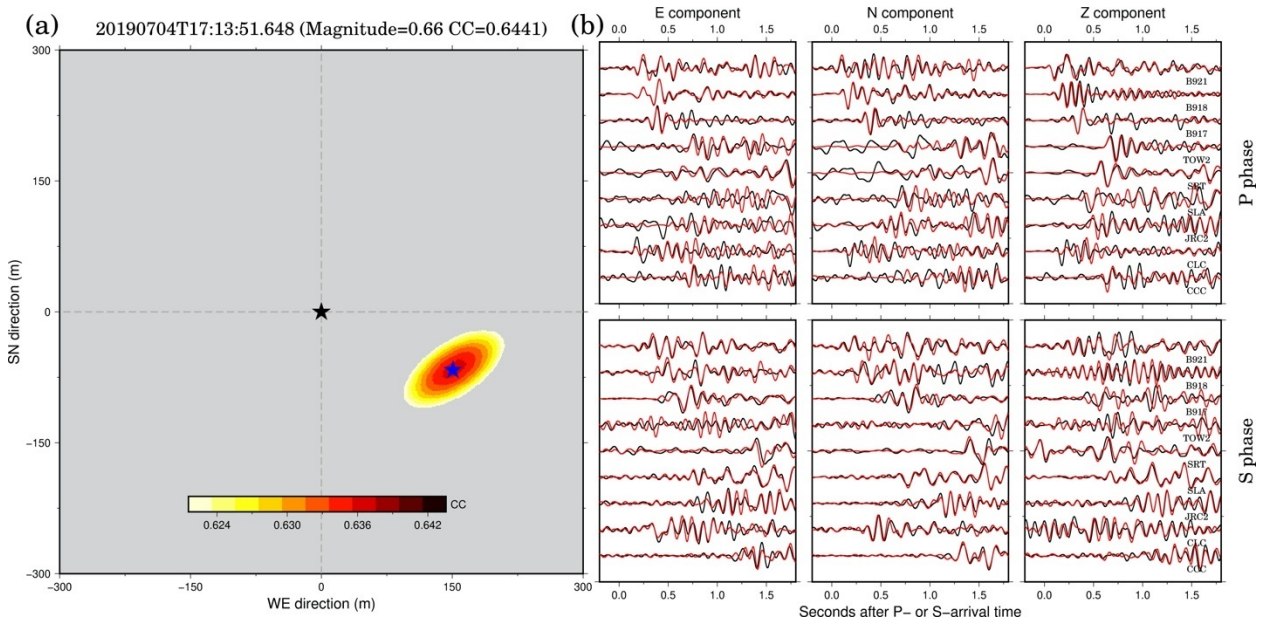


**Figures S26.** Smilar to Figure S5, but for EQ 23.

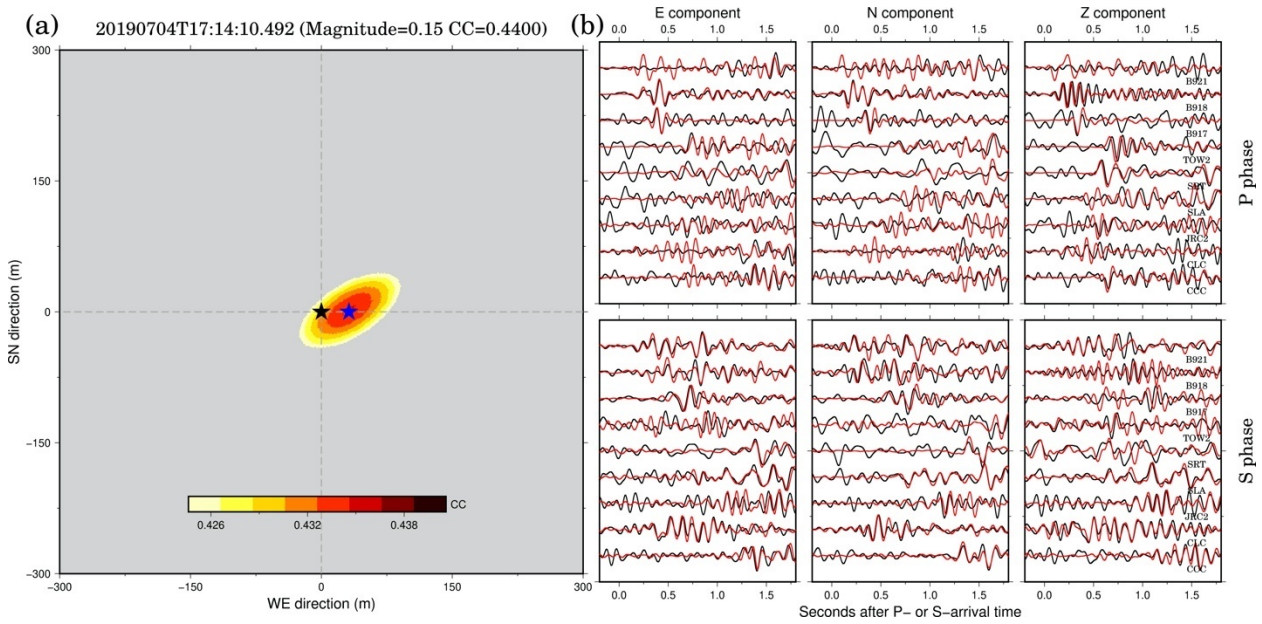


**Figures S27.** Smilar to Figure S5, but for EQ 24.

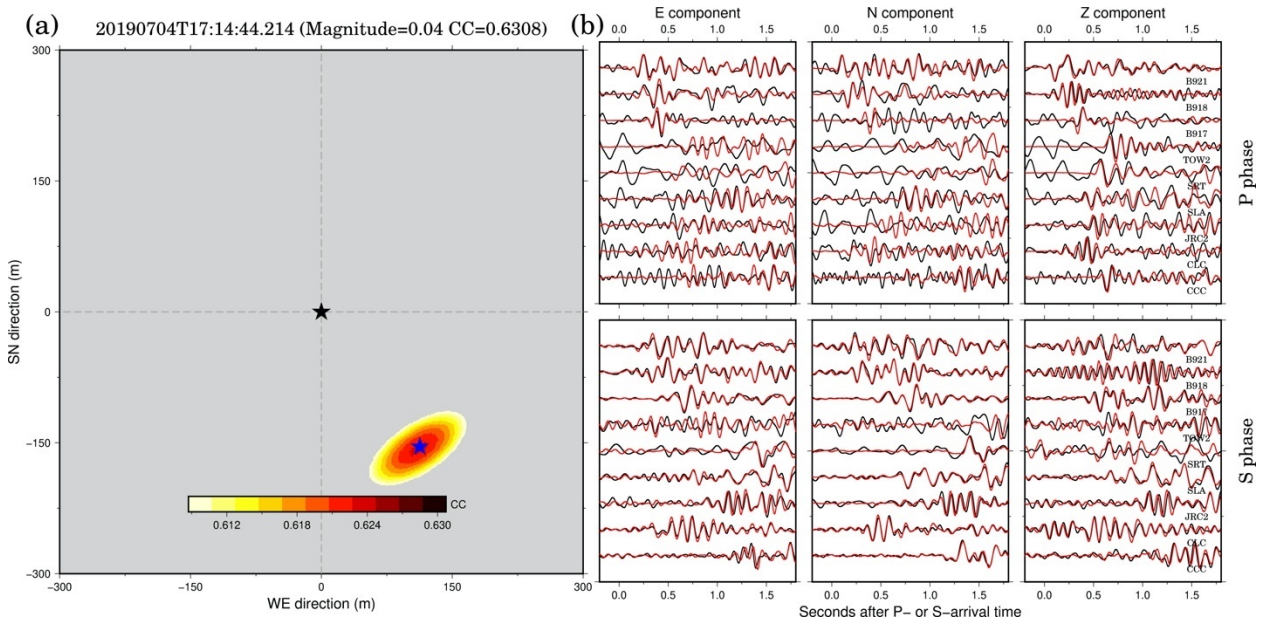


**Figures S28.** Smilar to Figure S5, but for EQ 25.

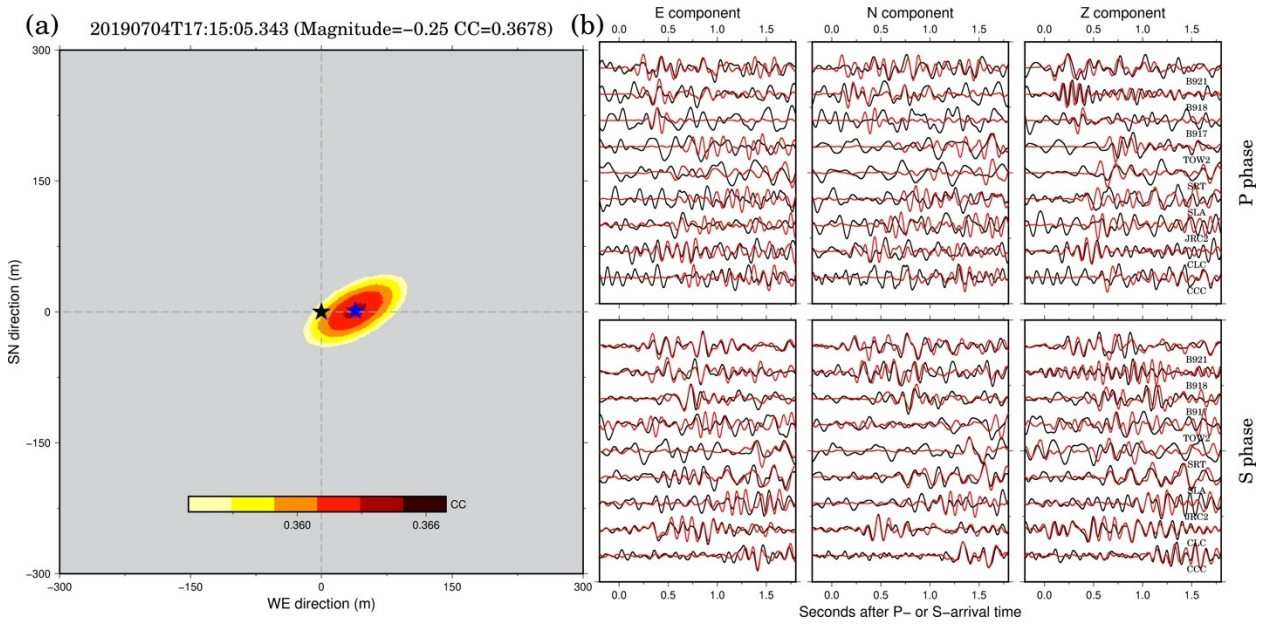


**Figures S29.** Smilar to Figure S5, but for EQ 26.

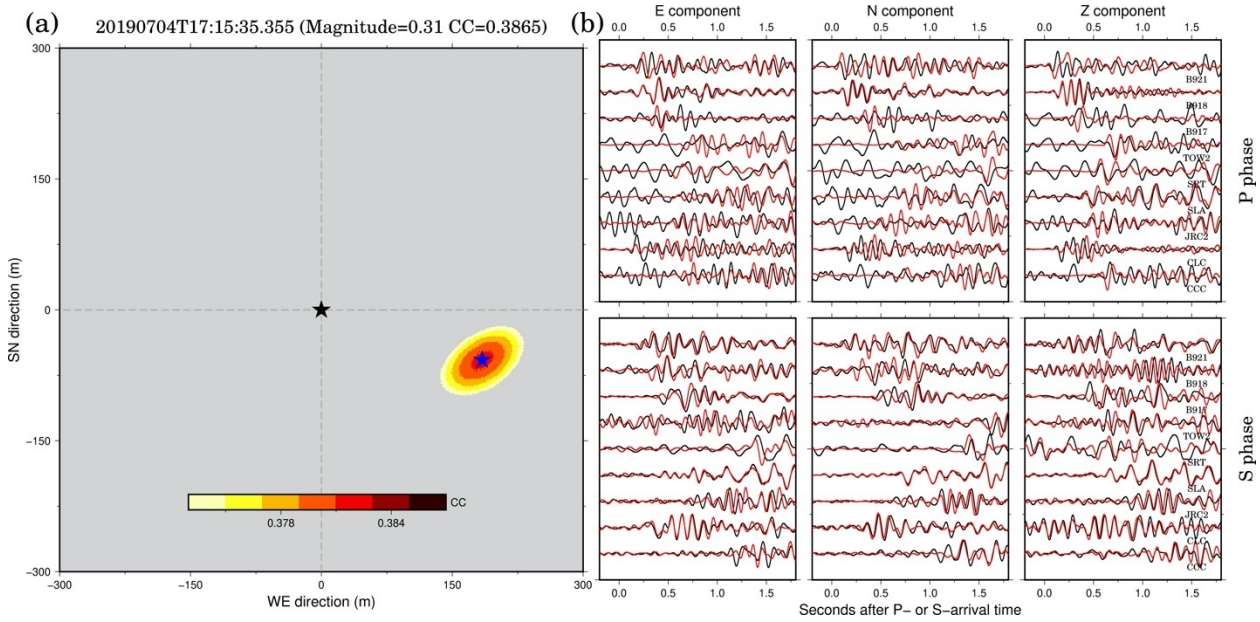


**Figures S30.** Smilar to Figure S5, but for EQ 27.

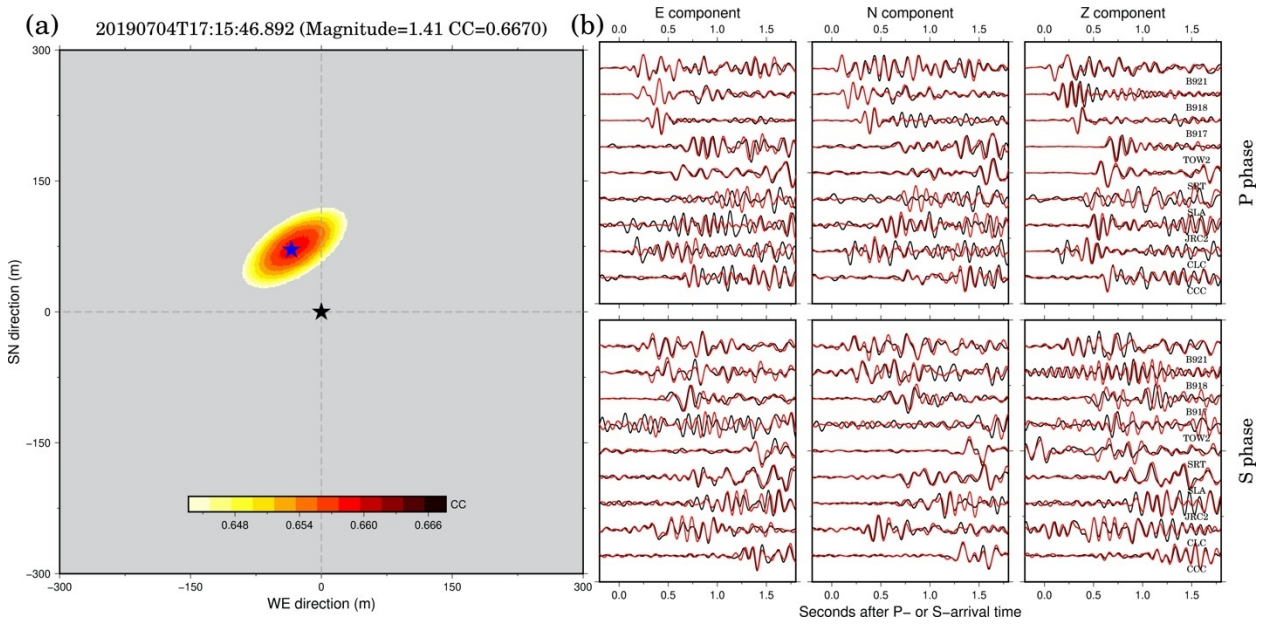


**Figures S31.** Smilar to Figure S5, but for EQ 28.

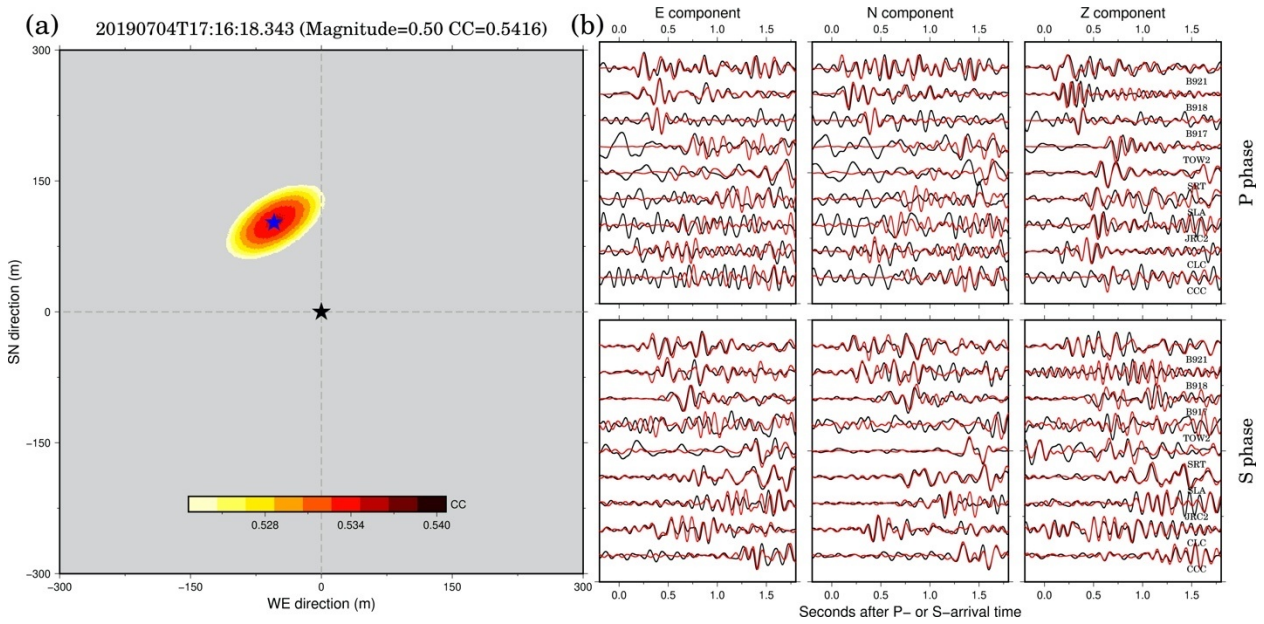


**Figures S32.** Smilar to Figure S5, but for EQ 29.

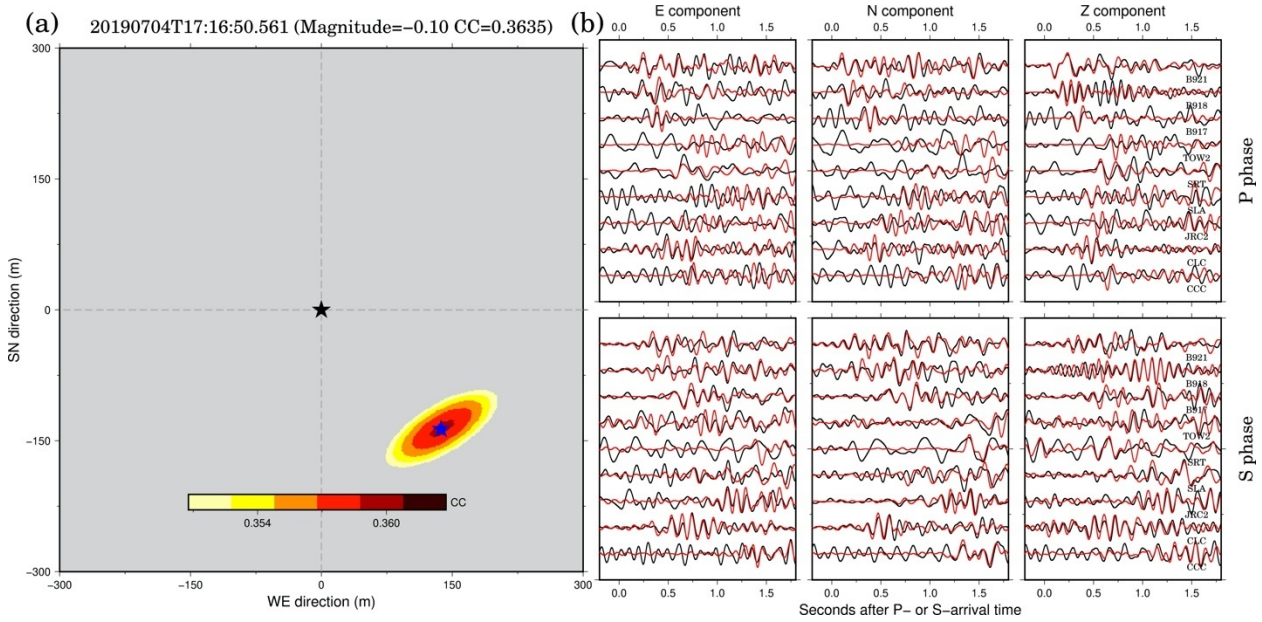


**Figures S33.** Smilar to Figure S5, but for EQ 30.

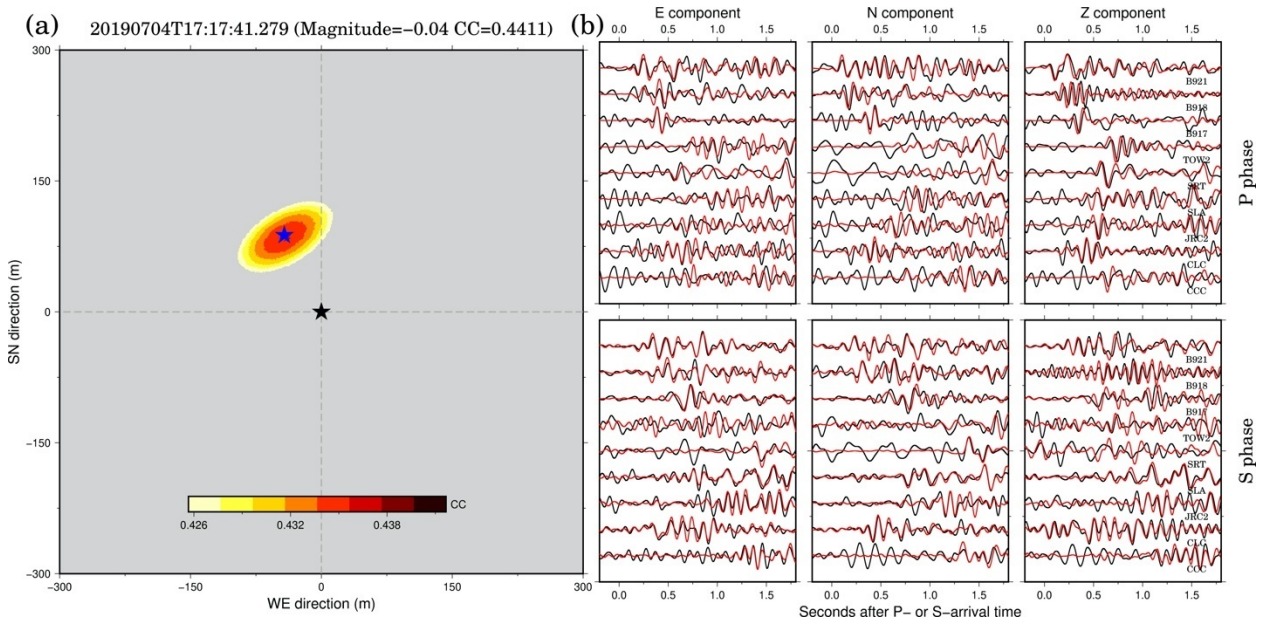


**Figures S34.** Smilar to Figure S5, but for EQ 31.

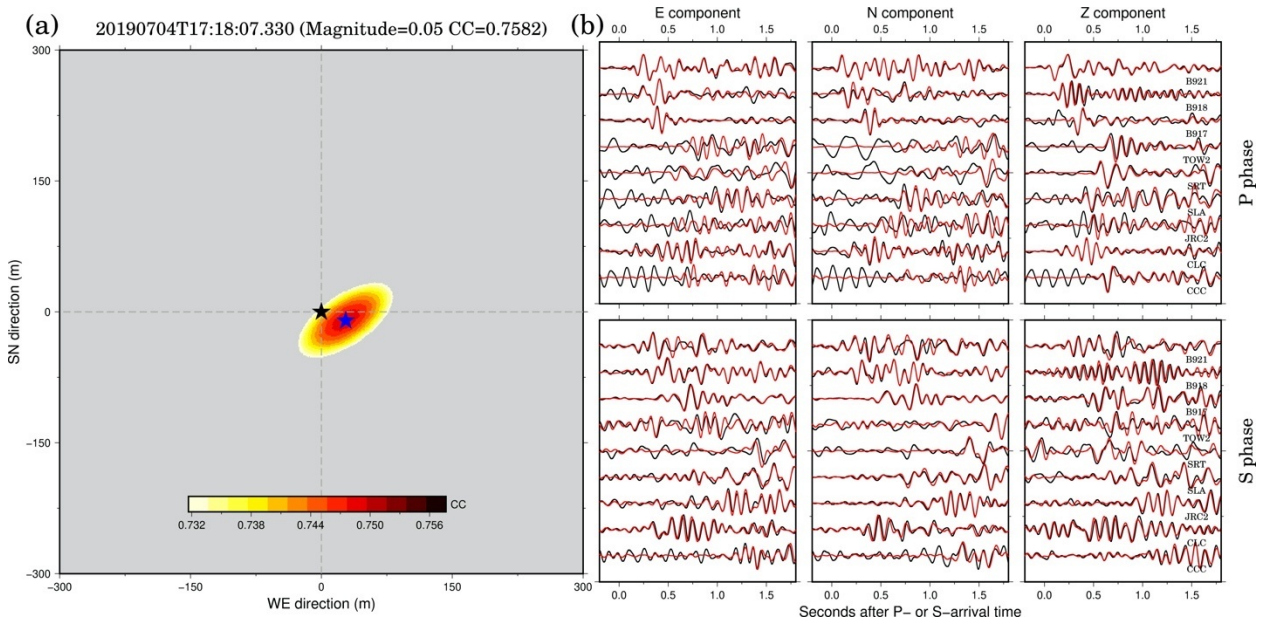


**Figures S35.** Smilar to Figure S5, but for EQ 32.

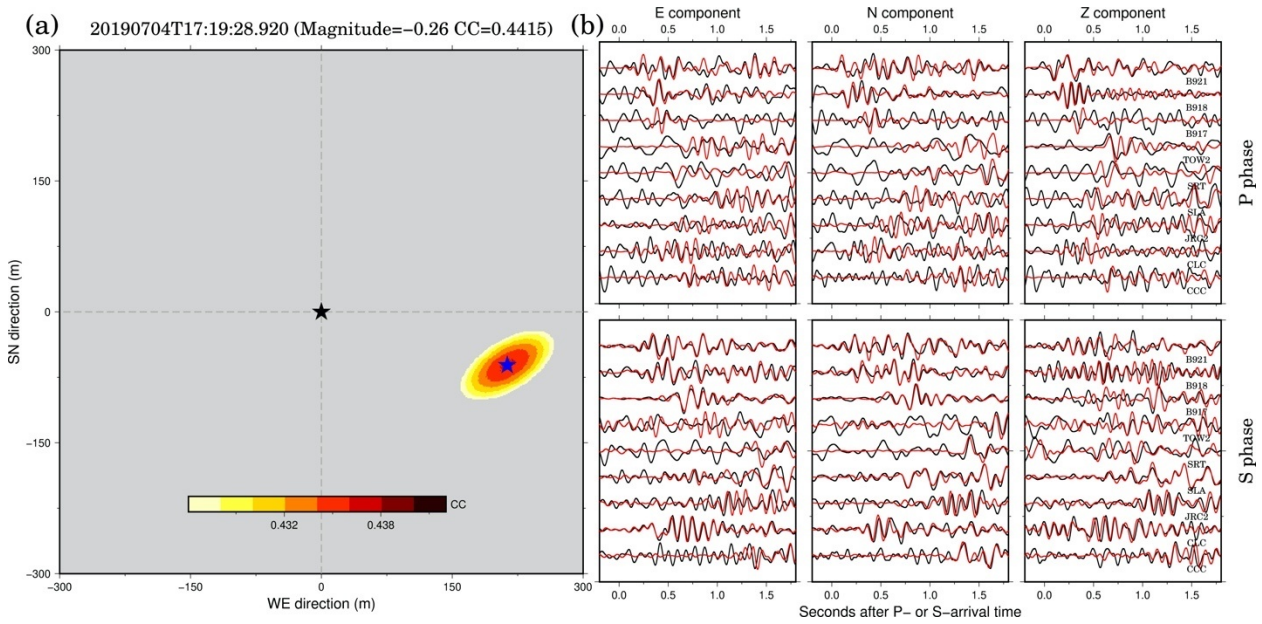


**Figures S36.** Smilar to Figure S5, but for EQ 33.

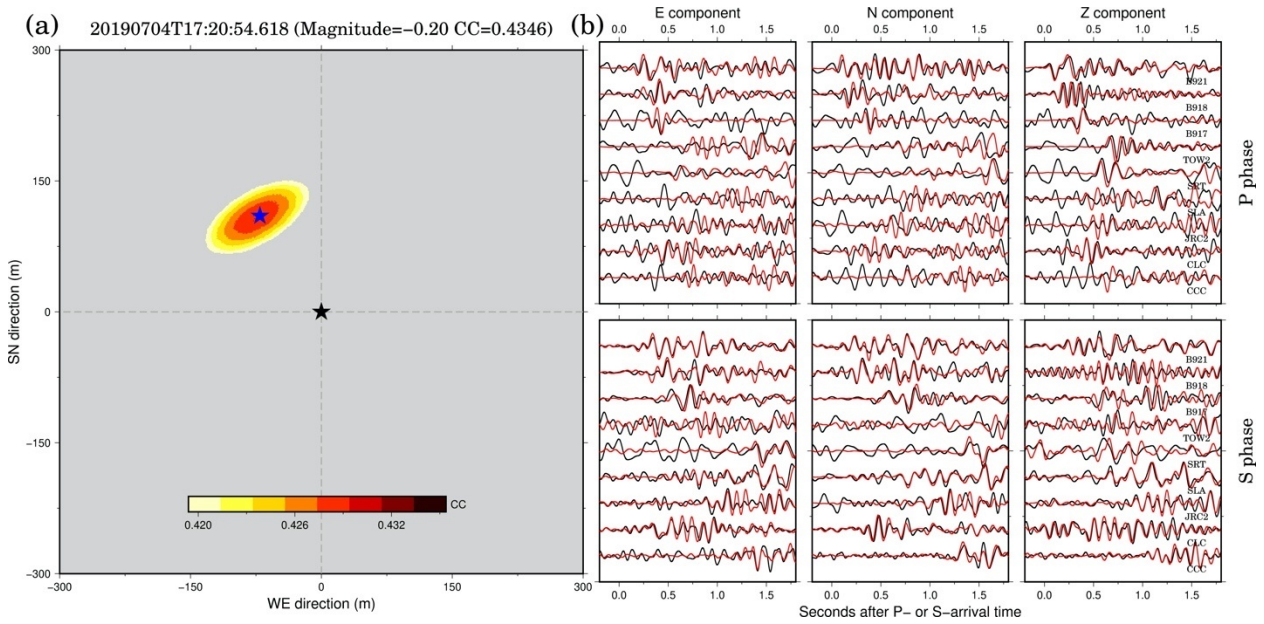


**Figures S37.** Smilar to Figure S5, but for EQ 34.

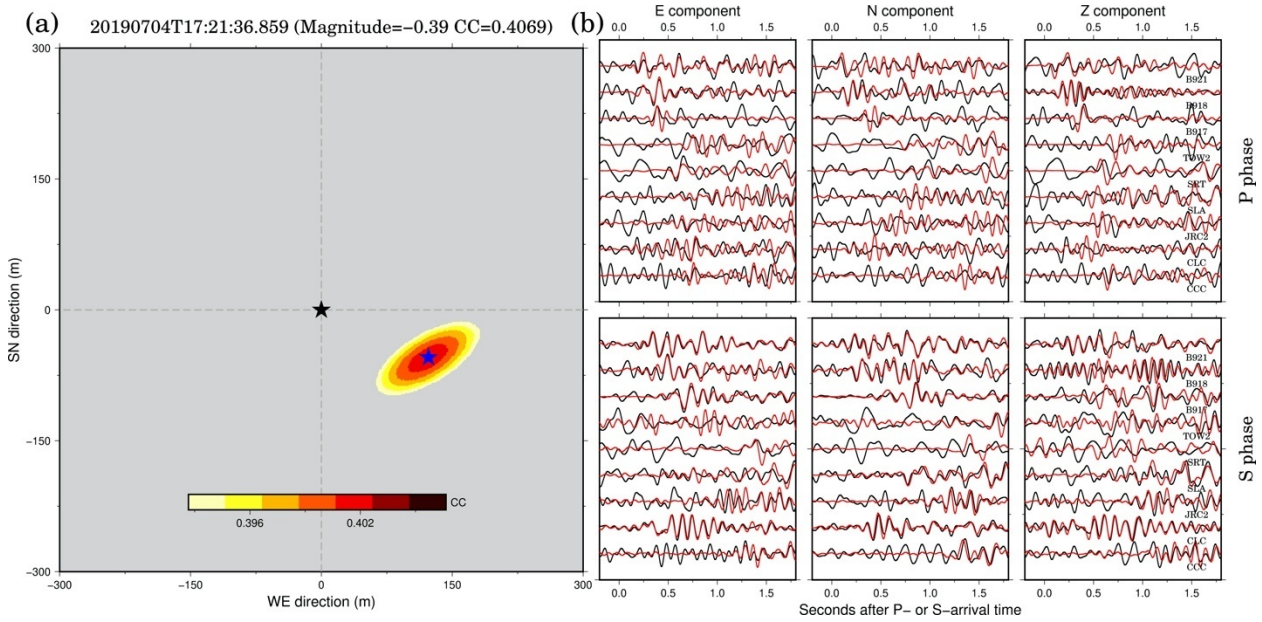


**Figures S38.** Smilar to Figure S5, but for EQ 35.

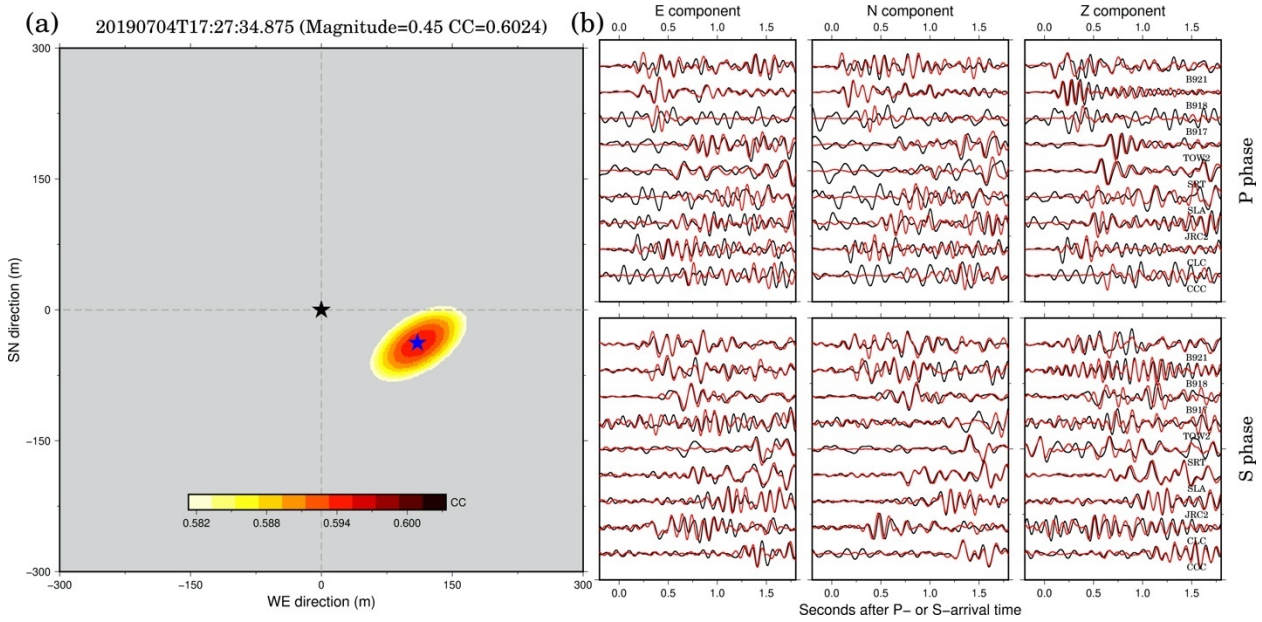


630

631 **Figures S39.** Smilar to Figure S5, but for EQ 36.

632
633
634
635
636
637
638
639
640
641
642
643
644
645

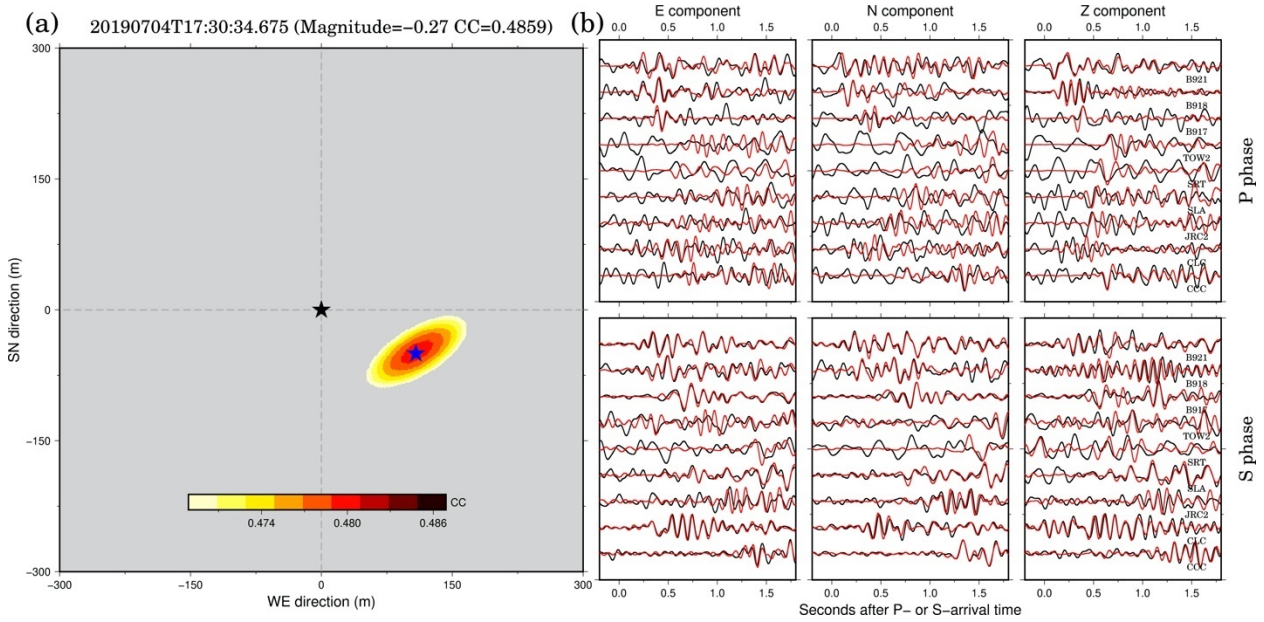


**Figures S40.** Smilar to Figure S5, but for EQ 37.

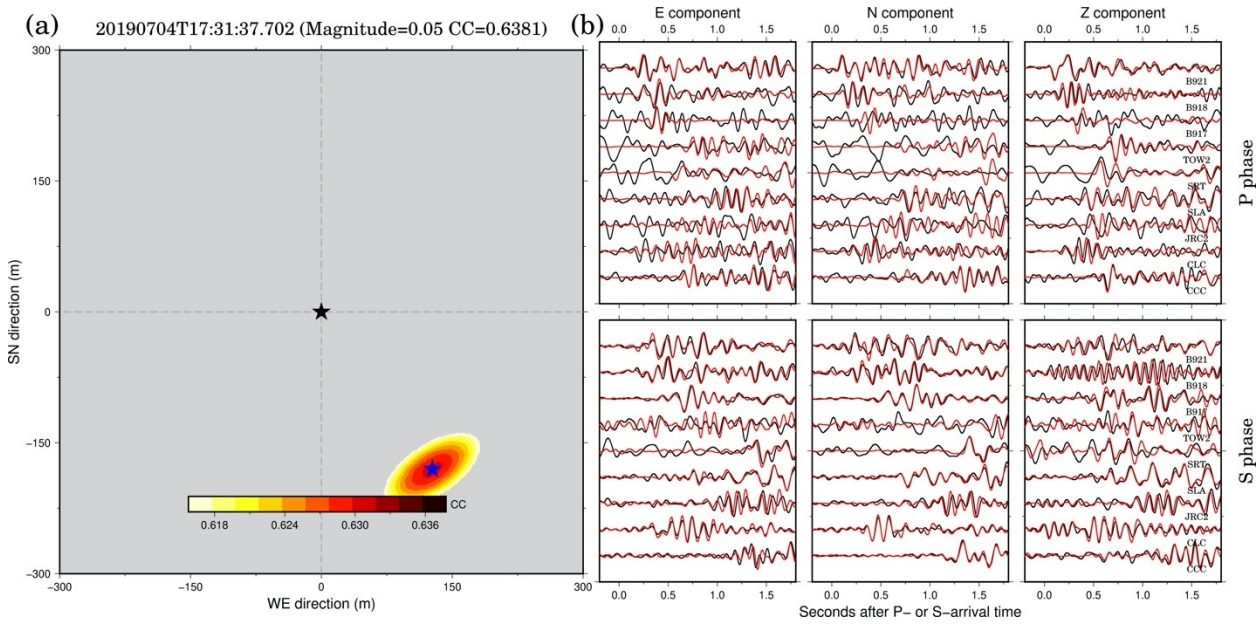


**Figures S41.** Smilar to Figure S5, but for EQ 38.

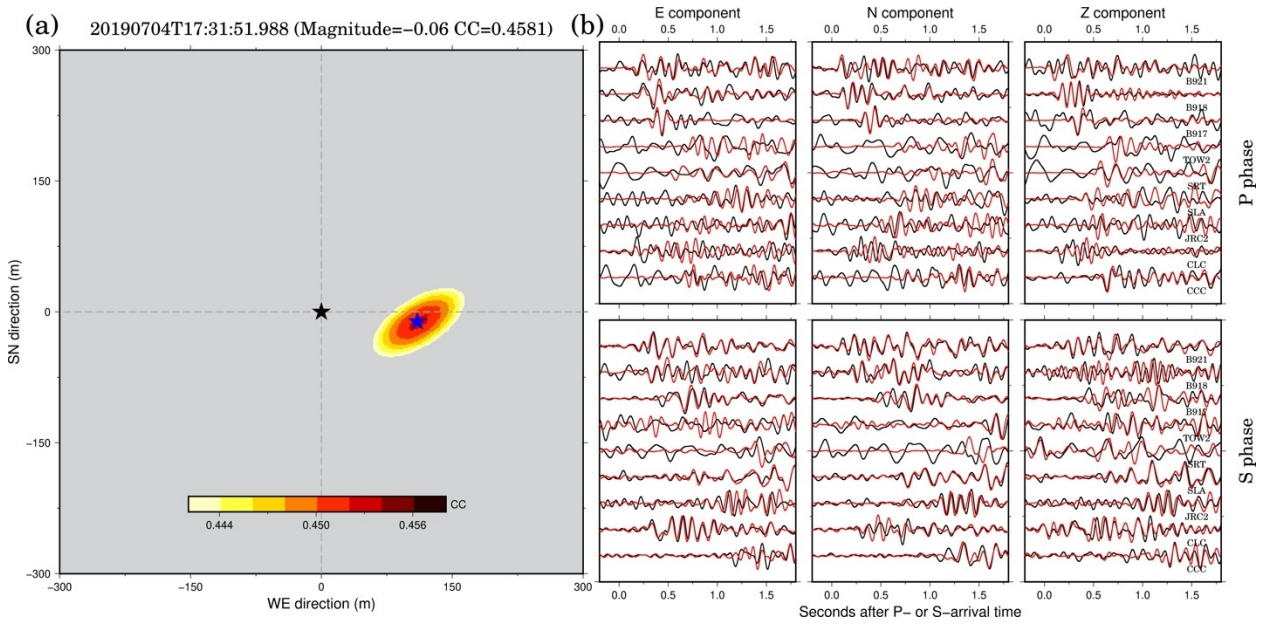


**Figures S42.** Smilar to Figure S5, but for EQ 39.

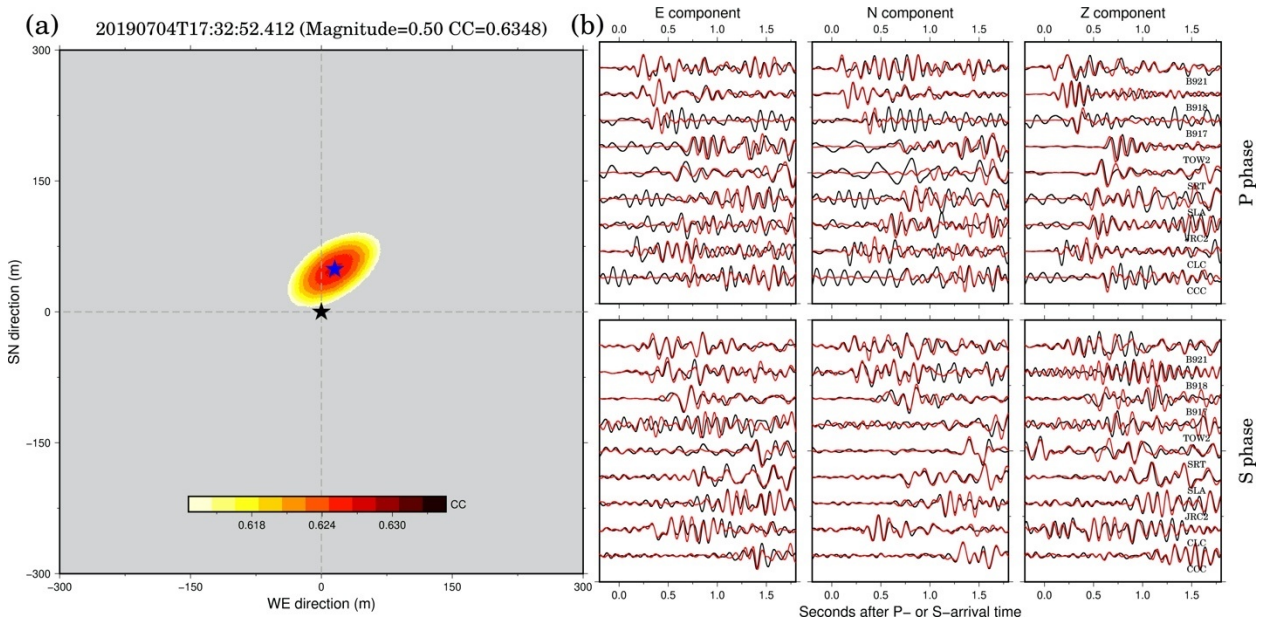


**Figures S43.** Smilar to Figure S5, but for EQ 40.

**Table S1.** The M&L foreshock catalog.

**Movie S1.** 3D movie showing detailed spatiotemporal distribution of these foreshocks listed in the M&L catalog (also see Figure 2).